UCLA
UCLA Electronic Theses and Dissertations

Title

Development and Testing of Two Lab-Scale Reactors for Electrified Steam Methane Reforming

Permalink

Author

Richard, Derek Michael

Publication Date

2021

Peer reviewed|Thesis/dissertation

UNIVERSITY OF CALIFORNIA

Los Angeles

Development and Testing of Two Lab-Scale Reactors

for Electrified Steam Methane Reforming

A thesis submitted in partial satisfaction

of the requirements for the degree Master of Science

in Chemical Engineering

by

Derek Michael Richard

2021

ABSTRACT OF THE THESIS

Development and Testing of Two Lab-Scale Reactors

for Electrified Steam Methane Reforming

by

Derek Michael Richard

Master of Science in Chemical Engineering

University of California, Los Angeles, 2021

Professor Carlos G. Morales-Guio, Chair

With increasing concern over the environmental impact of chemical manufacturing processes, a transition to synthesis methods that replace fossil fuel based processes with renewable electricity based processes is eminent. This work highlights the development of a high temperature proton conducting membrane reactor based on BZCY tubular membrane architecture which was designed and built to test the electrochemical SMR performance of BZCY membrane systems. Alongside this, an existing reactor system was retrofit to utilize Joule heating by applying an electric current directly through the FeCrAlloy reactor tube. CO_2

methanation and SMR tests were performed, and results was compared between Joule heating and external heating by a furnace. Joule heating showed improved methane conversion and reaction rates up to twice that observed when externally heated by the furnace. Together, these systems provide new capabilities for testing electric based SMR that will aid future research in the Morales-Guio group.

The thesis of Derek Michael Richard is approved.

Philippe Sautet

Panagiotis Christofides

Dante Simonetti

Carlos Morales-Guio, Committee Chair

University of California, Los Angeles

2021

Table of Contents

List of Figures

List of Tables

Acknowledgements

I would like to thank all of the individuals that have helped me in my learning, supported me in my pursuit of advanced graduate degrees, and provided me with motivation to continue this journey.

Most importantly I would like to thank my wife, Allison Glasco, who has supported me throughout this endeavor, cared for me when I forgot to take care of myself, and helped me to maintain focus on my long term goals. It is here love and support that has carried me through this degree.

I would also like to thank all the professors in the Chemical and Biomolecular Engineering Department at UCLA who have helped me along the way. I especially thank Professor Carlos Morales-Guio, who has patiently challenged me to grow in many ways throughout this process and has provided support and guidance for my research. I also thank Professor Dante Simonetti who has help guide this research, provided additional lab space and equipment, and has been helpful and encouraging throughout.

I extend my gratitude to all the members of the Morales-Guio Group, especially Jun Ke who contributed significantly to this research, and to Yu-Chao Huang who co-authored a literature review with me.

Finally, I am gateful for the support of my friends and family who have lovingly supported me and encouraged me throughout my time at UCLA.

1. Introduction

With advances in green electricity generation and increasing concern over the environmental impact of industrial processes, pressure to transition away from fossil fuel based manufacturing techniques is likely to reach a tipping point in the near future[1–4]. Electricity derived from solar and wind has reached a point at which it is cost competitive with conventional power generation systems[5]. In addition to cost incentives, renewable sources significantly reduce greenhouse gas (GHG) emissions for power generation compared to conventional sources. While renewable based electricity in 2020 only accounted for 21% of power generated in the US, renewable sources are predicted to become the dominant source of electricity before 2050 [6]. With increased availability and reduced cost of renewable electricity and the potential for future tax incentives to transition away from fossil fuels, the chemical manufacturing industry is likely to begin a transition towards electrified unit operations in the near future[1–4].

The initial shift to electricity will likely take form in the conversion from natural gas fired heating, to electrified heated. Combustion of natural gas is the primary method of providing heat to current processes due to the low cost (X) and abundance of this natural resource[7,8]. Methane (the primary component of natural gas) is also one of the most effective heat sources available, producing 891 kJ mol^{-1}. However, combustion with air, produces CO_2. As such, Industrial fired heaters used in the production of hydrogen alone are estimated to account for 1% of global CO_2 emission[7]. Additionally, the use of gas fired heaters requires extensive heat integration within chemical plants, necessitating large scale operations to be economical and reach high overall efficiencies[8–10]. Due to the potential for high impact[7] and the existing availability of mature technologies for power-to-heat transformations[11], electric based heating is likely to be a first step in the transition of chemical manufacturing to electric based methods.

1

While the higher cost of electricity compared to natural gas has dissuaded large scale implementation in the past[1,5,6,12], the many benefits of electric heating have been discussed extensively[7,11,13]. With previously discussed incentives to adopt electric based technologies, these advantages may finally be utilized in industrial processes. First, with the utilization of electricity sourced from renewables, Joule heated processes could eliminate GHG emissions produced by fired heaters. Additionally, utilization of electric heating for process heat would increase the thermal efficiency of these processes. In fired heaters, much of the energy produced is lost in the form of flue gas, as there is a limit to the amount that can be economically recovered by heat integration[8,9]. However, with Joule heating, energy is applied directly to the process fluid without the production of a flue gas that carries energy out of the process. Joule heating also provides improved thermal response resulting in more accurate temperature control and faster startup times[7,11,13]. Finally, if utilized in direct heating of reactor tubes, electric heating could improve catalytic activity by reducing the thermal gradient often present in packed bed systems providing more consistent heat to the process [7,14–18]. These advantages make Joule heating an obvious first step in the transition to electric based chemical manufacturing as electricity prices become competitive with natural gas.

Industrial utilization of electricity will likely begin with adaptation of existing systems to utilize Joule heating; However, future developments will likely yield entirely new chemical manufacturing processes that are based on electrochemical techniques. Some processes such as electrochemical production of hydrogen in electrolyzers are already reaching stages of development where they are competitive with conventional manufacturing techniques [5] These systems are inherently modular in nature and typically scale easily to a range of applications which could allow for decentralized production of chemicals and utilization of resources[3,19].

Electrochemical systems allow control over catalyst surface potentials, expanding the range of potential catalytically active materials[20–23], and allowing for reactions to occur at milder conditions than conventional technologies[24–28]. Additionally, proper design of these systems can allow for microscale integration of heat and mass transport to facilitate reaction and separation processes simultaneously[1,23,29,30]. While many of the electrochemical techniques to make industrially relevant chemicals are still in their infancy, this technology offers obvious advantages over conventional techniques, and significant effort are being placed into developing useful electrochemical processes[20].

In the development of these electrochemical processes, emphasis is often placed on developing technologies that eliminate the need to use fossil fuels as a feedstock. For example, the use of electrolysis, to split water into hydrogen and oxygen, has long been touted as the future end-all solution to making green hydrogen and a large sector of electrochemical research is focused on developing methods of converting CO_2 into carbon-based chemicals. However, the attention given to the development of these technologies tends to overlook issues related to implementing these technologies on a large scale. Electrolysis may produce emissions free hydrogen, but it is much more energy intensive than conventional steam methane reforming (SMR). This is demonstrated by comparing the standard enthalpy of reaction for electrolysis and SMR. Comparing **Equations 1** and **2** clearly shows the 245 kJ mole^{-1} energy advantage to making hydrogen from methane[31].

$$H_2O \rightarrow H_2 + \frac{1}{2}O \qquad\qquad \Delta H^o_{298} = 286 \ \frac{kJ}{mole \ H_2} \qquad\qquad \textbf{Eq. 1}$$

$$\frac{1}{4}CH_4 + \frac{1}{2}H_2O \rightarrow \frac{1}{4}CO_2 + H_2 \qquad\qquad \Delta H^o_{298} = 41 \ \frac{kJ}{mole \ H_2} \qquad\qquad \textbf{Eq. 2}$$
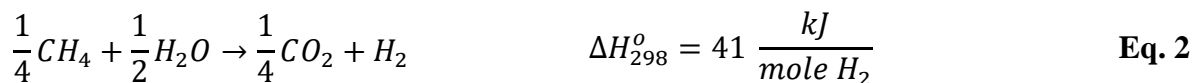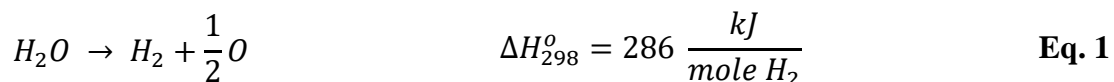
Additionally, SMR produces CO and CO_2 which can be utilized to make essential carbon-based precursors, such as methanol, that our society is reliant upon. To provide this necessary carbon feedstock, the popular opinion is to utilize CO_2 captured from air, but this technology is far from an economical point of development[32]. CO_2 captured from air is also inherently less efficient than utilizing the carbon byproduct of SMR due to the extremely low concentration of CO_2 in the atmosphere compared to the highly concentrated gas produced by SMR. Traditionally thought of as a dirty process, SMR accounts for approximately 3% of global anthropogenic CO_2 emissions[7]. However, if renewable electrification were to be implemented along with capture and utilization of the carbon products, SMR could be made emissions free and offer an energy advantage over alternative options. This thesis investigates the recent developments in environmentally friendly SMR and the intersection of conventional reactor technology with electrification. While alternative electrochemical techniques may take the lead in the future, electrification of SMR offers environmentally friendly solutions for the near term where immediate impact can be made on reducing the environmental impact of modern chemical manufacturing.

2. Background

2.1 Current Practices

In modern industrial chemical manufacturing processes, SMR is an integral source of hydrogen, CO and CO_2[33]. While the overall stoichiometric equation for SMR has been highlighted in **Equation 2**, in reality the overall reaction is achieved by the manipulation of two independent reactions. First is the reforming reaction which converts methane and steam into CO and H_2 as highlighted in **Equation 3**. The reforming reaction is then followed by the water gas shift (WGS) reaction which converts CO and steam into CO_2 and H_2 as outlined in **Equation 4**. The Reforming

4

reaction is highly endothermic, while WGS is slightly exothermic leading to an overall endothermicity. Conventional processes manipulate these two reactions to provide the desired ratio of CO and CO_2 for the conversion to other carbon based chemicals. This mixture of H_2, CO and CO_2 is called syngas due to its utility in synthesizing other chemicals. Because of the chemical building blocks that it supplies, SMR is an essential step in many processes that manufacture more complex precursor chemicals such as ammonia and methanol[1,2,7,34,35].

$$CH_4 + H_2O \rightarrow CO + 3H_2 \qquad \Delta H^o_{298} = 165 \frac{kJ}{mole\ CH_4} \qquad \textbf{Eq. 3}$$

$$CO + H_2O \rightarrow CO_2 + H_2 \qquad \Delta H^o_{298} = -41 \frac{kJ}{mole\ CH_4} \qquad \textbf{Eq. 4}$$
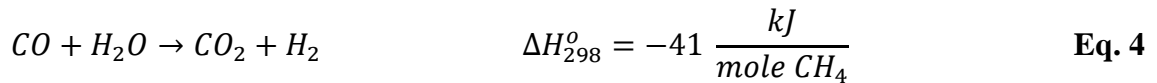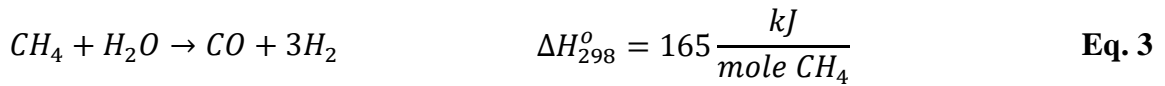
Methane, due to its symmetry, and resulting lack of polarity, is a very stable molecule that can be difficult to activate[20,22]. Many kinetic schemes have been proposed to describe the behavior of the SMR Kinetics, but it is commonly accepted that the rate limiting step is the activation of the first C-H bond[36–41]. To overcome the energetic barrier to activating this bond, highly active catalyst and high temperatures and pressures are required to convert methane at reasonable rates. Reformers typically rely on a Ni based catalyst that is supported on ceramic packing shaped to provide uniform flow, good mixing, and low pressure drop [42]. High heat flux at high temperature is necessary to balance the high endothermicity of the reaction and maintain temperatures necessary to reach reasonable reaction rates.

As such, reforming reactor tubes are mounted directly in the radiant section of a furnace where they operate at temperatures above 800°C. These reactors can come in a variety of configurations Including, bottom fired, top fired and side fired heaters relating to the location of burners. These furnaces are typically heated by combusting natural gas with air to provide 891 kJ

mol^{-1} methane. Consequentially, this also produces significant amounts of CO_2 which is typically vented to atmosphere[43]. Calculation of the thermodynamic minimum carbon contribution from the furnace indicates that at least 16% of the total carbon emissions can be attributed to providing heat for SMR. Considering inefficiencies in the process, this contribution could significantly increase for a real-world process. Clearly, elimination of this source of carbon emissions would significantly decrease the climate impact of SMR[7].

In addition to forming harmful gas that are released into the environment, there are other characteristics associated with fired heaters that make them less than optimal sources of heat for SMR. Due to the endothermicity of SMR, significant temperature gradients can form inside the reaction tubes, this reduces the activity of the catalyst near the center of the tube and can lower the equilibrium conversion [7,14–18]. The presence of these large gradients in temperature also contribute to the formation of coke in the catalyst bed that can reduce the catalyst active area[7,43]. Additionally, while a significant portion of the combustion energy is transferred in the radiant section to the reforming reaction, leftover energy is carried with the gas to the convection section of the fired heater. In this section other parts of the process are utilized to integrate the leftover heat, but the energy in the flue gas is never entirely recoverable[8,10]. Combined, these disadvantage of using fired heaters help to highlight where improvement would be most impactful for SMR.

2.2 Joule Heating

Joule heating, more commonly known as resistive heating, is a well-established alternative heating method that eliminates all of the previously mentioned issues related to using fired heaters for SMR. This heating method has long been used at smaller scales to provide heat for things like boiling water for coffee, electric stove tops, and central heating for houses. Joule heating is ideal for small scales where combustion heat would not be suitable to the application or were the

difference in cost between natural gas and electricity is less noticeable. At Industrial scales, natural gas is traditionally used because it has been significantly less expensive compared to electricity. However, with the increasing prevalence of inexpensive renewable based electricity, and the potential for carbon taxes as environmental concerns increase, electric based heating may become an attractive option [1,7,10,11,43].

The governing concepts associated with Joule heating are fairly simple, which helps to explain its widespread use. Power generation into heat is related primarily to current and resistance by **Equation 5**, which can be related to the generalized power equation $(P = I \times V)$ by the relationship between current and potential $(I \times R = V)$. By **Equation 5**, it can be seen that when driving a high enough current through a conductor with a given resistance, the heat generated will be proportional to the square of the current when the resistance is constant. Utilizing a material with a temperature independent resistance would then provide a relatively simple way of controlling exactly how much energy is input into a process. Perhaps the most attractive characteristic of resistive heating is the fact that it has a performance coefficient of 1.0, indicating that 100% of the energy put into the process is converted to heat[7,11].

$$Heat\ Rate = Power = I^2 \times R \hspace{3cm} \textbf{Eq. 5}$$

When compared to fired heaters, Joule heating offers clear advantages for use in industrial processes. First, this method of heating when paired with electricity supplied by renewable sources, does not produce any harmful by-products that could be released into the atmosphere. If used in place of fired heaters for SMR, joule heating would reduce the GHG emissions of the process by a minimum of 16%[7]. Second, the amount of heat provided to a process can be easily controlled and quickly manipulated simply by adjusting the current. This would make startup times significantly shorter due to the instantaneous effect of joule heating and make adjustments during

7

operation nearly instantaneous. Third, reactor tubes could potentially be used as joule heating elements themselves. This would eliminate the temperature gradients observed across the radiant section of the furnace and across the wall of the reactor tubes providing more certainty and control over the conditions in the catalyst bed[7]. Additionally, this could significantly reduce the size of the reactor since there would be no need for a large furnace body[11]. Lastly, research outlined in the results section of this thesis indicate that using a DC power source to supply the power for joule heating, may increase catalytic activity in joule heated reactors. Judging by the advantaged presented here, the characteristics of Joule heating offer clear benefits for use in industrial heating when compared to fired heaters.

2.3 Washcoating

While Joule heating could be used for traditional packed bed reactor designs, using a washcoat has been suggested as a possible alternative that would be better suited to joule heating. The technique of washcoating has long established uses such as in catalytic converters that use washcoated monoliths. In Joule heating a thin layer of porous catalyst support could be coated on the reactor tubes internal surface. This support could then be impregnated with catalyst, providing a uniform catalyst dispersion along the length of the tube. Since the catalyst layer is in direct contact with the heats source, the temperature gradient within the active area of the reactor is eliminated ensuring uniform and controllable reaction temperatures. Obviously in larger tubes this would not be an ideal arrangement due to the reduced catalyst surface to volume ratio. However, Joule heating would allow for more flexibility in reactor design and washcoating could be optimal for use with smaller tubes or joule heated monoliths.

The potential of combing Joule heating with washcoating was highlighted by Wisemann et. al. who demonstrated successful application of this combination to electrify SMR. In their work,

a FeCrAlloy tube was selected as the reactor body and joule heating element due to its relatively temperature independent resistance. A 130 µm thick Zn based washcoat was applied to the tube and then impregnate with Ni to act as the catalyst. Results showed catalyst utilization of 20%, which is much higher than typically observed for traditional heterogeneous catalysts for SMR and showing the potential to reach 65% utilization with optimization of the washcoat thickness. The promising results of this publication inspired much of the washcoated reactor research presented in this thesis and were used as a basis for the design of the joule heated reactor system.

2.4 Ceramic Based High Temperature Electrochemical Reactors

Although seemingly unrelated, the recent development of proton conducting ceramic membranes capable of operating at high temperatures, has provided new opportunities for the application of Joule heating and electricity to SMR[29,44,45]. These membranes are based on a $BaZr_{0.8-x-y}Ce_xY_yO_{3-\delta}$ (BZCY) architecture that shows highly selective conductivity for protons that reaches useful rates of 10 mS/cm at 800°C and 1 bar of steam pressure[1]. The conductivity of this membrane is highly temperature and humidity dependent requiring high temperatures for adequate conductivity. While the temperature dependance may limit its applications, it is ideal for SMR which favors high temperature reaction conditions.

The design of a reactor around this membrane takes the shape of a membrane electrode assembly. In the center is the membrane which is sandwiched between two porous catalyst layers. In the porous catalyst layer, NiO catalyst particles are mixed with BZCY ceramic to provide conductive connections to the membrane while allowing gases to reach the catalyst surface. In the designs previously studied, tubular membranes where used, where the anode was on the inside of

the tube and the cathode on the outside[1]. The structure of these tubular membranes and their

catalyst layers is presented in **Figure 1**.
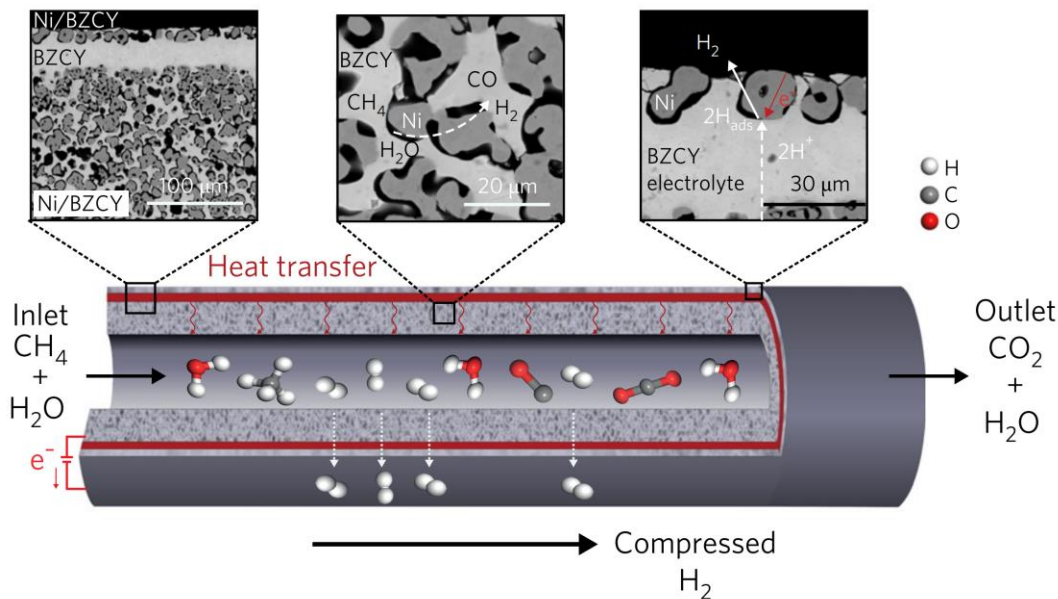
Figure 1. A schematic of a tubular proton conducting membrane reactor for SMR. SEM images from left to right, show a cross section of the MEA, detail of the anode catalyst layer, and detail of the cathode catalyst layer on the BZCY electrolyte. Adapted from ref. X with permission from Springer Nature, Copyright © 2017

Methane and steam are introduced to the Anode, where they react to form CO_2 and protons.

Due to an electrical potential applied across the membrane, the protons are then electrochemically

pumped to the Cathode on the outside of the tube where they form into high purity hydrogen gas.

The ability to electrochemically pump hydrogen to high pressure is benefit of the tubular

architecture of the ceramic membrane. If the membrane designed in a planer orientation, any

pressure differential would risk fracturing the brittle ceramic membrane. However, ceramics are

well suited to compressive forces like those associated with the compressed hydrogen stream on

the outside of the tube pressing in. While the natural concentration gradient between the sides of

the membrane acts to oppose the separation of hydrogen from the reacting gases, application of an

electrical potential provides the ability to overcome the chemical potential created by this concentration gradient. As a result, the degree of separation and compression can be modified by simply adjusting the electrical potential applied across the membrane.

A byproduct of the electrochemical separation and compression is the generation of heat within the membrane. The equations governing the generation of heat for each of these processes are given in **Equation 6** and **7**. Upon inspection it is obvious that these two equations are essentially the same as the joule heating equations, but instead of resistance to electron transport, the resistance for separation comes from the membrane's resistance to proton transport and the resistance for compression comes from the concentration (or partial pressure) gradient across the membrane[1,23,46].

$$Power\ for\ Separation = U_{sep} \int_0^t I\ dt = R_{cell} \int_0^t I^2 dt \qquad \text{Eq. 6}$$

$$Power\ for\ Compression\ = U_{Nernst} \int_0^t I\ dt = \frac{RT}{2F} \ln\left(\frac{p_{H_2}{}^{II}}{p_{H_2}{}^{I}}\right) \int_0^t I\ dt \qquad \text{Eq. 7}$$

As a result, operating conditions can be adjusted to optimize the microthermal heat integration and essentially eliminate energy loss within the system.

Additionally, the separation of hydrogen from the anode shifts thermodynamic equilibrium to enhance the reaction, enabling high methane conversion and selectivity for CO_2 over CO[1]. The result is a highly concentrated CO_2 product on the anode and high purity compressed hydrogen on the cathode. Clearly the high level of microscale integration within this type of system allows for significant reduction in external heat integration and the overall complexity of SMR. This could be ideal for smaller scale applications such as decentralized production of hydrogen from methane

11

at hydrogen fuel cell filling stations. With reduced electricity costs, this technology could soon be highly competitive with conventional SMR techniques.

The technology and concepts of this process could be applied to production of other chemicals as well. For example, a similar system was tested for use as an electrochemical Haber Bosch process to make ammonia. In that system the cathode catalyst was replaced with a Vanadium-Nitride catalyst and nitrogen gas was fed to the cathode. Hydrogen and nitrogen then combined to make ammonia at a rate of 1.89×10^{-9} mol/cm^2/s and a faradaic efficiency of up to 15% at ambient pressure[19,26]. This is one of the best results to date for an electrochemical ammonia synthesis process. The results of both applications show promise for future development in this area but many information gaps remain to be filled. The design section of this thesis details the design and fabrication of a system designed to test the types of system described in the past few paragraphs. While no testing was conducted for this thesis, future plans are in place to utilize this system to gain a deeper understanding of how these BZCY based SMR systems function and what their limitations are.

3. Experimental design

3.1 Selection of Parts and Design of Simple Heating Experiments

Initial experiments demonstrating efficacy for direct joule heating of reactor tubes, were designed to confirm successful heating of the reactor tube by application of a controlled current. Electrical, and thermal safety where key concerns addressed in the design of the system used for these experiments. Also of importance was the selection of an appropriate power supply and reactor tube material. This section discusses the considerations that were made when designing this experimental setup.

The first consideration when designing this experiment was the material to be use for the reactor tube. Previous publications suggested that a FeCr-Alloy tube would be well suited to our applications[7]. This alloy was primarily chosen because its electrical resistance was relatively independent of temperature and it was highly oxidation resistant up to 1100°C. It also provided a high enough resistance to produce the required heat at attainable currents. Tubes used in this work were acquired from Goodfellow with dimensions of 500mm length, 6mm outer diameter, 5.4mm inner diameter and composition of 72.8% Fe, 22% Cr, 5% Al, 0.1% Y, and 0.1% Zr. The manufacturer provided resistance was 134 µOhm cm. The hardness of the material caused initial concerns about the ability of Swagelok fittings to create gas tight seals with the reactor tubes. However, it was found that the thin wall design of these tubes provided adequate reduction in resistance to deformation so that compression fittings could seal as intended.

Electrical connections to the tubes were made with custom fabricated copper brackets that allowed contact with a large surface area of the tube to minimize contact resistance. Initially 3mm thick copper was used but was found to be to rigid to provide good contact with the tube. 0.6mm thick copper was finally used to make these brackets with stainless steel M10 bolts used to connect electrical cables from the power source. 1 AWG copper welding cable was used to provide the current from the power source with minimal resistance. Sense lines were also connected at the copper brackets for the power source to detect the current flow and voltage drop between the brackets on the reactor.

For initial heating tests, 6 inches of stainless steel tubing were connected to the ends of the heated tube to provide mounting points far enough from the heated portion as to prevent melting of any of the mounting fixtures. The stainless-steel tubes were wrapped with electrical tape near the end of the tube where they were fixed inside clamps to hold the assembly above the bench as shown

13

in **Figure 2**. This electrical insulation provided electrical isolation to prevent the formation of any unwanted outside circuits that might affect the results. Initial tests at low temperatures used a thermocouple attached to the outside of the insulated tube with Kapton tape. A layer of Kapton tape was maintained between the probe and the tube to prevent interference by the voltage drop along the tube with the thermocouple reading. Later Unitherm ceramic fiber insulation was used

Figure 2. Initial Joule heating test setup in fume hood.

to reduce heat loss at higher temperatures and stainless-steel shielded k-type thermocouple were inserted under the insulation from each end. No interference with the thermocouple reading was. detected even with direct contact with the tube. The Entire assembly was placed inside a fume hood to minimize points of access and reduce risk of unintended contact with the assembly that could potentially cause harm to personnel in the lab or the assembly. However, the power source was places on a table outside the fume hood to allow ease of access during operation

This electrical insulation prevented the formation of any unwanted outside circuits that might affect the results. Initial tests at low temperatures used a thermocouple attached to the outside of the insulated tube with Kapton tape. A layer of Kapton tape was maintained between the probe and the tube to prevent interference by the voltage drop along the tube with the thermocoup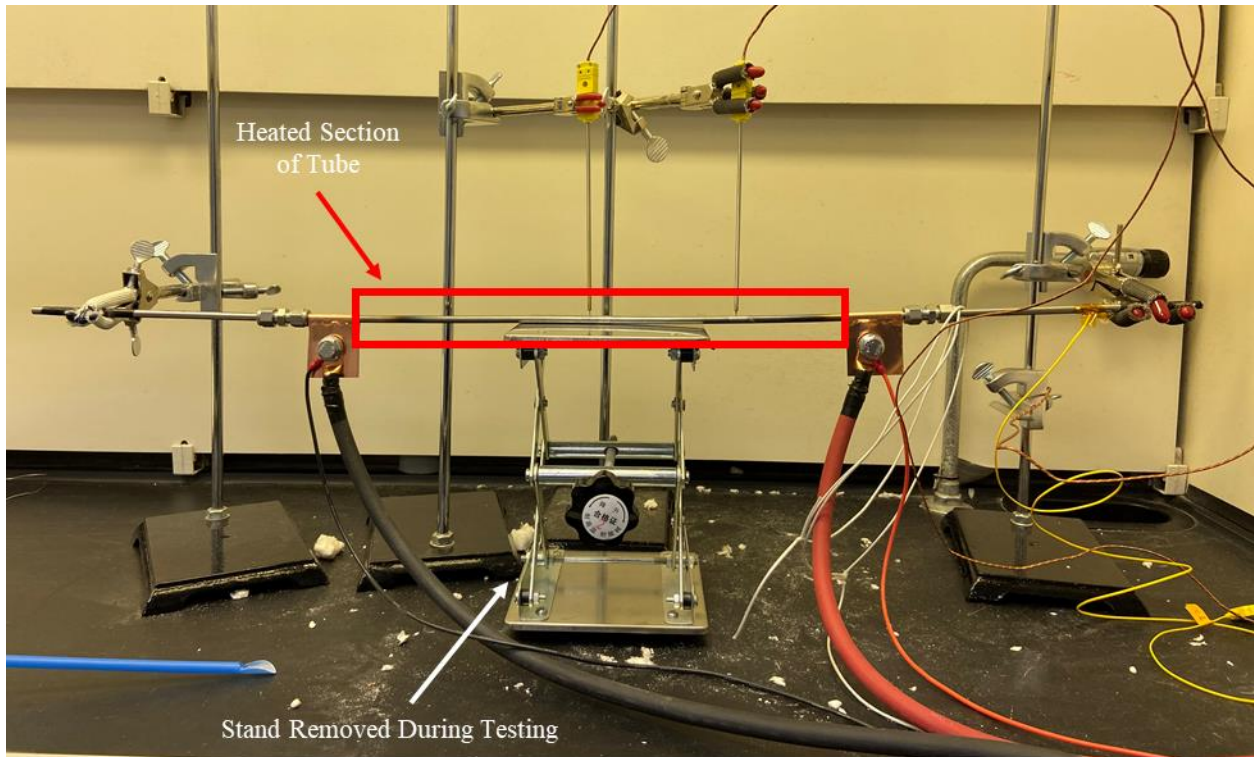le reading. Later Unitherm ceramic fiber insulation was used to reduce heat loss at higher temperatures and stainless-steel shielded k-type thermocouple were inserted under the insulation from each end. No interference with the thermocouple reading was detected even with direct contact with the tube. The Entire assembly was placed inside a fume hood to minimize points of access and reduce risk of unintended contact with the assembly that could potentially cause harm to personnel in the lab or the

In previous investigations, a variable transformer had been used to supply power to the reactor tube. However, we decided to use a DC power source to allow for more precise control over the current in joule heating experiments as well as to act as a future power supply for the electrochemical type reactors being developed. Using the governing equations for Joule heating and heat transfer with insulation, it was determined that a power supply capable of providing approx. 80A would be required to reach the highest temperature we might wish to achieve. A programmable DC power supply (Chroma model 62012P-40-120) capable of supplying up to 40V, 120A, and 1200W was selected as an adequate instrument capable of providing the high accuracy power required for all experiments being considered.

3.2 Modification of Existing Externally Heated Reactor System

Testing of reactions was conducted in a pre-existing system in Dante Simonetti's lab intended for high temperature reactions. This system provided the capability to control multiple gas feeds, temperature of the gas lines, steam injection, and used an electric furnace to control the

reactor temperature. The attached furnace would be used to provide external heat to control measurements with existing packed bed catalysts. However, during Joule heating type experiments, it was simply used as thermal insulation for the reactor tube and to measure the temperature of the reactor. A PFD of the system can be seen in **Figure 3**.
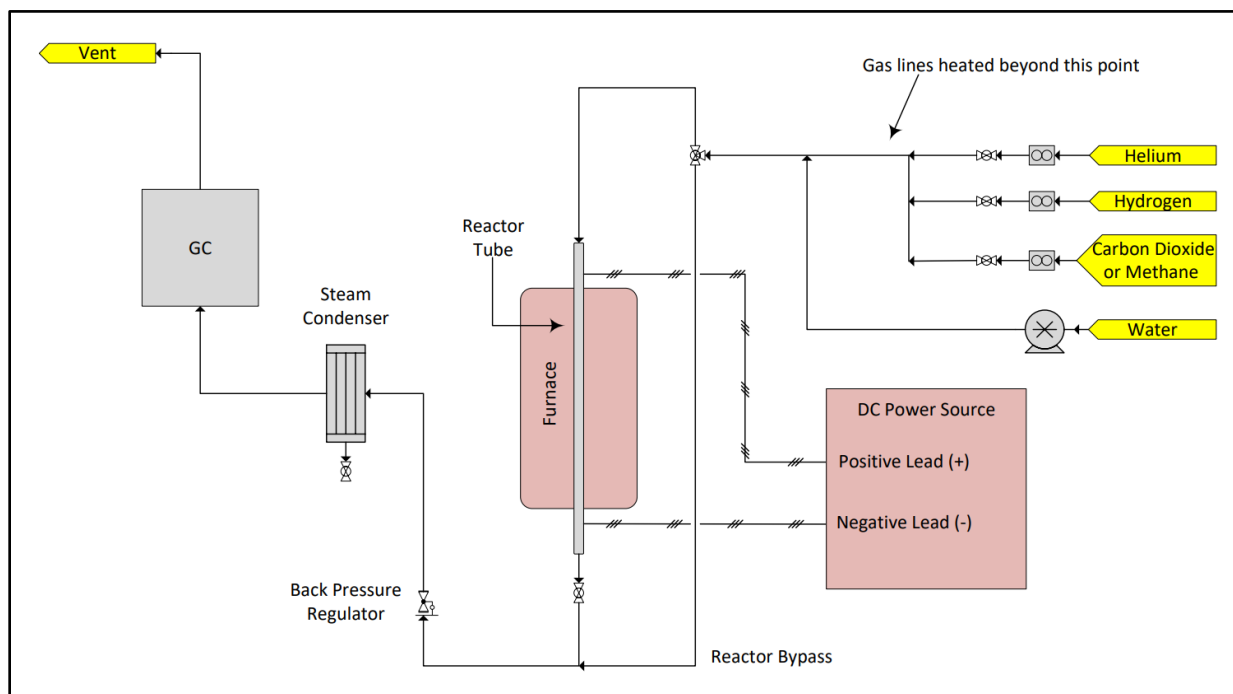
Figure 3. A process flow diagram of the Joule heated reactor system.

Although the system was pre-existing, several modifications were made to enable the use of joule heating. Upon initial inspection it was found that the Joule heating tubes were slightly longer than the reactor tubes usually used in the system, thus the tubing was adjusted to account for this and to center the joule heating tube in the insulation of the furnace. The added length of the Joule heated tube allowed for the connection of the copper brackets to be outside of the furnace body while keeping the majority of the tube well insulated. While the tube was well insulated, it was found in initial temperature tests that much higher currents where required to reach similar

16

temperatures as when insulated in the initial heating tests. It was determined that external circuits were primarily to blame.

To remedy the problem a section of PTFE tubing was inserted in the bypass line to prevent the creation of a less resistive circuit through the bypass around the reactor. This significantly improved the performance of the Joule heating. Dielectric fittings where also introduced to minimize the possibility of sending current though external connections to the system such as the mass flow controllers or the gas chromatograph. This addition added slight improvement in addition to isolation of the bypass. Upon installation of these fitting, the PTFE tubing and ensuring that all mounting points where electrically insulated, the system performed nearly as well as the initial heating experiments. Any deviation was attributed to differences in insulation since all electrical causes had been eliminated.

3.4 Design and Fabrication of PCMR

In parallel to the research conducted with Joule heating, a reactor system was designed and built for the purpose of testing high temperature electrochemical methane-based reactions. While the electrochemical system would be similar to the Joule heated reactors in the use of electrified heating, the general requirements for the electrochemical system required a configuration that could not be supported by any existing systems. As a result, an entirely new system was designed to facilitate the future experiments planned for this electrochemical system that will be referred to as the proton conducting membrane reactor (PCMR).

At the core of the PCMR is a proton conducting BZCY ceramic tube that is coated with a catalyst on both sides and mounted on a half inch diameter 24cm long alumina tube. For the future experiments planned for this system, SMR would be conducted on the inside of the tube at the

Anode while hydrogen would be electrochemically pumped to the cathode on the exterior of the membrane. At the cathode hydrogen would be either captured as high purity hydrogen gas or reacted with other chemicals. To facilitate the function of this cell a configuration had to be devised to introduce controlled gas flows to each side of the tube independently, make efficient electrical connections to each electrode from outside the gas tight system, and provide supplemental heat.

Design of the PCMR began with consulting literature. Because similar systems had been tested previously as discussed in the background section, information from these studies was taken into consideration. Additionally, schematics for previous systems were obtained from the membrane supplier, CoorsTek, that aided in deciding on the final design of the reactor. While special consideration in the design will be discussed, a picture of the assembly presented in **Figure 4** as well as the parts list in **Table 1** should be referenced for specifics of the Swagelok components that were used.

Starting from the feed side of the reactor, a K-type thermocouple is inserted at the center of the system to measure the temperature of the feed entering the membrane. Next the anode feed enters through a tee connected to a 3/16" nickel tube that introduces feed gases to the far end of the membrane. Around this nickel tube is the membrane attached to the ½" alumina riser. The end of the riser is attached to another tee that allows the anode effluent to exit the reactor. In this way, feed is preheated as it flows through the nickel tube, reverses directions at the far end of the membrane, and then flows past the membrane in the annular space between the membrane and the nickel tube. Nickel wool is also placed in the annular space between the nickel tube and the membrane to allow for electrical contact between the two surfaces. By this arrangement, an electrical connection can be made to the anode by simply connecting to the exposed portion of the nickel tube on the outside of the reactor.

As shown in **Figure 4** the membrane and most of the Alumina riser are contained in ¾" SS tubing between two tees that provide cathode feed and effluent access. On the left side of the reactor an oxygen free copper rod is inserted into the reactor shell through Swagelok fittings. This copper rod acts as the external point of electrical connection for the cathode. On the inside of the cell 0.025mm oxygen free copper wire is wrapped around the membrane to act as a current collector. This wire is connected by a 0.5mm oxygen free copper wire to the copper rod. Dielectric fittings are utilized on each feed and effluent line to prevent external circuits form forming and the lumina tube provides electrical insulation between the two sides of the membrane.
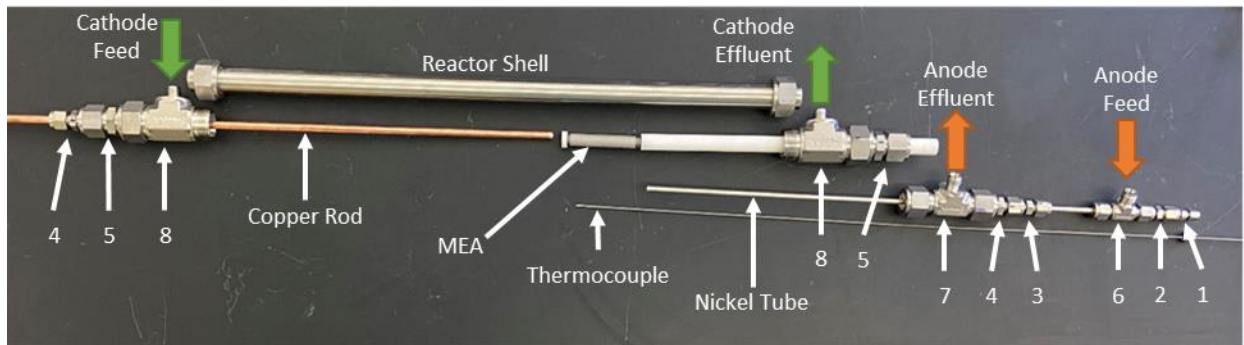
Figure 4. A picture of the PCMR internals with labeled Swagelok parts corresponding to **Table 1.**

Table 1. A parts list for the Swagelok fitting used in the PCMR.

Part#	Swagelok Part#	Quantity	Description
1	SS-100-R-2	1	1/16" Tube Fitting X 1/8" Reducer
2	SS-200-R-3	1	1/8" Tube Fitting X 3/16" Reducer
3	SS-300-R-4	1	3/16" Tube Fitting X 1/4" Reducer
4	SS-400-R-8	2	1/4" Tube Fitting X 1/2" Reducer
5	SS-810-R-12	2	1/2" Tube Fitting X 3/4" Reducer
6	SS-300-3-3-4	1	TEE, 3/16 X 3/16 X 1/4
7	SS-810-3-8-4	1	TEE, 1/2" X 1/2" X 1/4"
8	SS-1210-3-12-4	2	TEE, 3/4" X 3/4" X 1/4"

To enable the system to work with readily available Swagelok fittings, a few modifications were needed. First, several fittings were modified to remove the bump stops allowing the thermocouple, nickel tube, and alumina riser to pass entirely through the fitting. These are noted

in the parts list in **Table 1**. Additionally, due to the hardness of alumina compared to stainless steel, standard Swagelok ferrules would not make gas tight connections to the alumina riser. Typical Swagelok ferrules slightly deform the tubing on which they are installed to form a gas tight seal, but likely would have broken the alumina tube if installed similarly. Instead, PTFE ferrules were used to make the connections to the alumina riser. These soft ferrules provided an adequate solution. However, care had to be taken to ensure that they were spaced far enough from the furnace as to not exceed the safe working temperature of PTFE (Approx. 200°C). Besides these modifications, custom tees were ordered from Swagelok to provide ¼" connections for the feed and effluent gas lines. While these custom parts were not necessary, they provided several benefits including greatly reducing the number of Swagelok fitting needed to make these connections, reduced the number of possible leak points, and reduced the overall weight and size of the system.

Although the PCMR is the heart of the system, many ancillary pieces of equipment were also required. Gas flows were controlled with mass flow controllers as shown in the PFD (**Figure 5**). However, steam was injected by syringe pumps feeding deionized water into the gas lines. All gas lines where heated to 120-140°C to prevent condensation and provide heat for vaporization of the injected water. To prevent water interfering with the gas chromatograph used to analyze the reactor effluent, a condenser was installed before the gas chromatograph to collect the post-reaction steam. Additionally, a tube furnace was centered around the PCMR so that the membrane was positioned in the center of the furnace and a back pressure regulator was used to analyze the reactor effluent, a condenser was installed before the gas chromatograph to collect the post-reaction steam. Additionally, a tube furnace was centered around the PCMR so that the membrane was positioned in the center of the furnace and a back pressure regulator was used to adjust the system pressure in the PCMR. Altogether, this system would allow for precise control over the

20
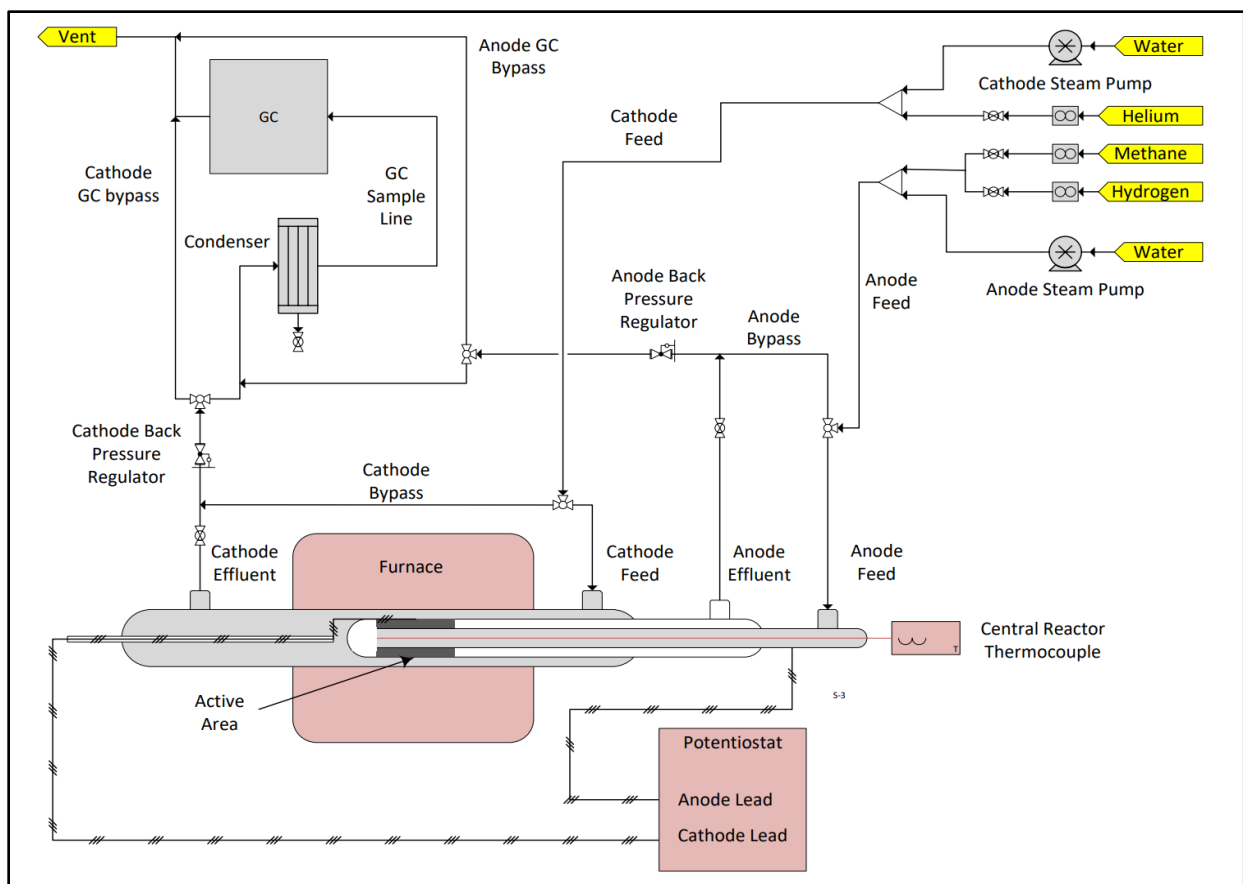
Figure 5. A process flow diagram of the PCMR system.

electrical load, gas flow rates, temperature, and pressure of the system enabling testing under a wide range of conditions and well suited to the planned experiments.

4. Experimental Methods

4.1 Initial Heating Tests

Initial Joule heating experiments were conducted in the simple system previously described as well as in the furnace used in the following experiments. The purpose of these experiments was to verify the ability to control the temperature of the reactor tube by driving a current through it and to become familiar with the operation of the Joule heating system as it is the first time that such a system has used in the Morales-Guio group. Initial tests were done in a fume hood with no insulation. Next a Unitherm, alumina-

silica insulation was added to minimize convective heat loss in the fume hood. This set of experiments allowed much higher temperatures to be reached and significantly lowered the current required to reach these temperatures.

Upon successful demonstration of Joule heating on the basic system, Joule heating was conducted without catalyst, with and without gas flow, in the furnace used for the following experiments. In these test, operating parameters were compared to those of the insulated basic system in the fume hood, and adjustments such as the addition of electrical insulation components in the gas tubing system were made to reach better agreement between the two systems. While the system was tested with and without gas flow, this was done only to verify previous calculations that suggested the heating of gas would have negligible effect on the temperature of the tube at a given current. As the energy required to heat the feed gas is less than 0.5% of the total heat being supplied by the tube, it was considered to have negligible effect. Testing showed no effects caused by the gas flow and such will not be discussed further.

4.2 Packed Bed Type Experiments

All Packed bed type experiments were conducted using the Joule heating system previously described in the design section using the same FeCrAlloy tube. Between experiments, this tube was cleaned thoroughly with deionized water and by scraping with a stainless steel rod that fit inside the tube. After scrubbing with the rod and rinsing with deionized water, multiple passes with a clean paper wipe were made to ensure that remaining residue was removed. This process was repeated until the cleaning wipe showed no signs of residue and visual inspection of the tube showed a shiny interior of the tube.

Upon ensuring cleanliness of the reactor tube, a small pea size wad of quarts wool was inserted to the center of the tube. This quartz wool acted as the porous and inert support to keep the catalyst in place. Catalyst was weighed and inserted into the tube using standard weighing paper. Once inserted, the tube was tapped on a hard surface to ensure the quarts was holding the catalyst in place and to let it settle. A steel rod was also used to tap the sides of the tube to help the catalyst settle in place to ensure homogenous gas

flow across the catalyst during testing. Finally, another pea size piece of quartz wool was placed on top of the catalyst to help hold it in place.

Two separate catalysts were used: one to provide a baseline comparison to industrial available catalysts and another representative of the synthesized catalyst in the washcoat that would be used in separate experiments. The baseline catalyst used was a commercially available nickel oxide SMR catalyst (HiFUEL R110, Alfa Aesar, 40% nickel (II) oxide and 60% aluminum oxide). This catalyst came in the form of large pellets that had to be ground to a desirable size to fit in the FeCrAlloy tube but was otherwise unmodified. The Washcoat simulant (WCS) catalyst was prepared using 99% purity ZrO_2 powder with 5μm particle size from Millipore Sigma as the support. 3g of Zr powder was mixed with 20ml of deionized water and 2.908g of Nickel Nitrate (nickel (II) nitrate hexahydrate, ≥97% purity, Millipore Sigma) and stirred for two hours. Solids were filtered out of the solution and dried at room temperature for 24 hours before calcinating in air at 500°C for four hours. Both catalysts were ground and sieved to similar particle sizes with an upper limit of approximately 0.1mm.

Reactor tubes loaded with catalyst were mounted inside the a furnace (Applied Test Systems, series 3210-75-8-12) as shown in **Figure 3**. During initial testing, the catalyst bed was observed to shift to the bottom of the tube and out of the hot zone of the reactor. To prevent this, a small stainless steel rod was placed inside the reactor to brace the catalyst bed in the center of the tube. When conducting Joule heating, the positive lead of the power source was attached to the feed side of the reactor tube (the top) and the negative side was attached to the product side (the bottom). To measure the temperature of the reactor tube, a K-type thermocouple was attached to the outside of the reactor tube at the location of the catalyst with high temperature tape. While previous work showed interference with the temperature measurement may be caused by the potential gradient along the tube, no issues were observed the method discussed here. This was tested using multiple thermocouples at varying orientations of attachment and comparison to a thermocouple in close proximity too, but not in contact with the tube.

23

Catalyst pretreatment under a Hydrogen atmosphere was conducted using heat provided by the furnace due to the automated temperature control it provided, and flowrates were set using mass flow controllers (MKS Instruments, G-series). Accuracy of the mass flow controllers was verified with a bubble meter and recalibrated if needed before each experiment for all gases used. During these system checks, the gases were run through a bypass line to prevent interaction with the catalyst. Once correct flowrates were confirmed and temperatures stable, the gas flow was redirected through the reactor tube and reduced in a gas flow of 15 SCCM H_2 (99.999% ultra high purity, HY UHP200 from Airgas) and 45 SCCM He (99.999% ultra high purity, HE UHP200 from Airgas) at 650ºC for one hour.

After reduction, gas flow was again directed to the bypass, switched to the flowrates for the desired test, and allowed to stabilize. Stability was tested by examining the response of an Agilent Technologies 7890B gas chromatograph (GC) over multiple injections and checking for consistency. Once stability was confirmed, the gases were switched to run through the reactor and monitored with the GC. GC calibration curves for the expected gases were conducted separately to enable quantitative analysis of the product stream.

Two different types of tests were conducted. First CO_2 methanation was conducted to become familiar with the system operations at lower temperatures and allow any issues to be addressed under safer conditions than those required for SMR. The gas flows utilized for CO_2 methanation experiments were 30 SCCM He, 30 SCCM H_2, and 15 SCCM CO_2 (medical grade, CD USP50, from Airgas). Methanation was conducted at 350ºC, 450ºC and 550ºC without backpressure. The second set type of experiment was SMR with flow rates 30 SCCM He, 15 SCCM CH_4/Ar (90.0% CH_4, balance Ar, AR ME90ZC-K from Praxair), and 22µL H_2O (deionized). Liquid water was inserted in the preheated feed lines using a New Era Pump Systems syringe pump. Preheat in the feed lines provided the heat to vaporize the water and prevent condensation until post reaction where it was collected in a condenser before reactor effluent entered the GC.

A few distinctions should be made regarding how the experiments were conducted. First, for CO_2 methanation with the Hi-Fuel catalyst, Joule heating was used. However, when CO_2 methanation was done with the WCS, heat was provided by the furnace. Hi-Fuel was tested for both furnace heating and Joule heating. During SMR experiments with Hi-Fuel, data suggested that Joule heating may be affecting the reaction. Therefore, in the following experiment where the WCS was tested for SMR, a combination of furnace heat and Joule heating was utilized in the same experiment. In this experiment, samples were measured for both furnace heating and joule heating. For each temperature, the furnace would be used to adjust the temperature of the reactor and then a set of injections would be taken. Following these samples, the furnace would be turned off and heat would be supplied by Joule heating. Injections would be taken while the reactor was being Joule heated and then heating would be switched back to the furnace which would be used to adjust to the next temperature. This process was repeated for each temperature tested. For temperatures that showed little activity, a minimum of two injections were taken for comparison to ensure the effluent was semi-stable. Temperatures that showed high activity were tested for multiple injections until changes in GC response appeared to become stable. While these tests give an idea of how the effluent changed over time, they were not intended as long-term stability tests and were not carried out to a point where true stability was reached.

4.3 Washcoated Reactor System

Wash-coated reactor based experiments were conducted with identical conditions to those outlined in the packed bed experiments. This was done to allow direct comparison between the two systems. Primary differences between the washcoated reactors and the packed bed reactor is that the washcoat usually covered the entire length of the tube, while the packed bed was only in a small fraction of the tube. This translates to a longer residence time for the washcoated type reactors. Fabrication of the washcoated reactor tubes began with application of the support to the inside of the tube. The previously mentioned Zr powder was mixed with 20mL of deionized water and pH corrected to a value of 4 by addition of 0.1 M nitric acid. After stirring for two hours to ensure adequate mixing, the solution was poured into the FeCrAlloy tube which

was sealed at the bottom with a valve. The solution was allowed to drain very slowly from the bottom of the tube after 2 hours by adjusting the valve. The tube was then allowed to dry for 24 hours at room temperature before calcining in air at 500ºC for four hours. Multiple layers were added to achieve the desired loading by repeating the process just described.

Catalyst addition was done by wet impregnation of the washcoat. Similar to how the washcoat was applied, a 0.5 M nickel nitrate solution was added to the tube. This was left to sit for 2 hrs giving the nickel time to adhere to the Zr washcoat. After 2 hours, the solution was drained, and the tube was dried identically to the Zr washcoat. The majority of work done with the wash coated reactor system was conducted by Jun Ke who has outlined the details of this work in his thesis. As such, this work will only be referenced in context of comparison to the packed bed system and is mentioned in this work only to aid the reader in understanding the context of the experiments discussed here.

5. Results

5.1 Initial Joule Heating

Initial testing of Joule heated tubes was done with a control system in a fume hood without insulation. The results from this test (not shown) indicated the need for insulation to reach the desired temperatures, so Unitherm, a commercial alumina-silica insulation was wrapped around the tube to reduce heat losses. Based on rough calculations for insulation thickness and heat loss, insulation was wrapped to a thickness of 2 inches. this thickness proved to be adequate to reach the desired highest temperature of 500ºC while remaining well within the limitations of the power supply. A temperature vs. current curve was generated from the measurements taken with the initial setup and used as a baseline for comparison. This data was fit with a second order polynomial equation to predict the behavior of the temperature with changes in current. This curve and its predicted behavior are shown in **Figure 6** data set (**A**). By plotting voltage vs. current, the

approach to ideality could be examined. This was possible due to the fact that with a constant

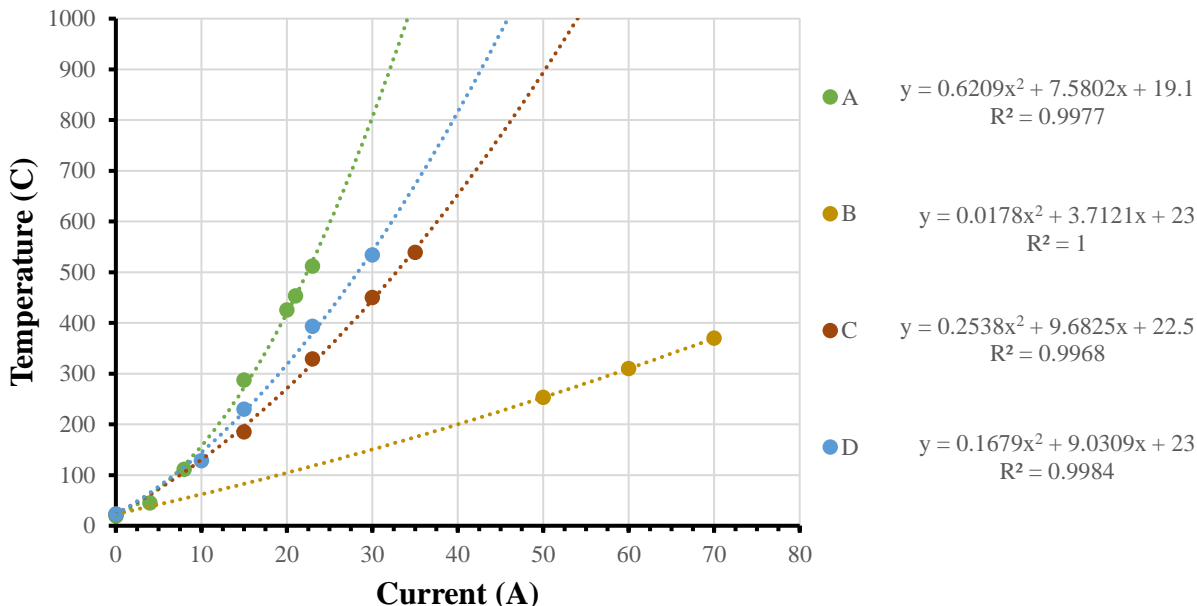resistance, there is a linear relationship between voltage and current where the resistance is the

Figure 6. Temperature vs. current curves for the control **(A)** and the reactor system without modification **(B)**, with PTFE bypass line **(C)** and with dielectric fitting **(D)**.

slope (**Figure 7**). It was found that the resistance shown by this curve for data set A showed a

resistance of 0.114 Ohms which is very close to the manufacturer provided resistance of 0.095

Ohms. Deviation is likely to be from contact resistance of the copper cable connections to the tube.

Further testing was conducted while the reactor tube was installed in the furnace body used

in the reaction tests. Data set **(B)** shows initial test of the system without any modification and

clearly has a lower resistance than that shown by the initial tests in the control system (data set

(A)). Since the furnace body was well insulated, this resistance difference had to be from the new

system. It was determined that the gas bypass line was likely the largest contribution to the

deviation in resistance. To resolve this issue a section of the stainless steel line use for the bypass

was replaced with PTFE tubing. Data set **(C)** shows the results after this modification. There is a

significant increase in the resistance indicating that the bypass was providing a low resistance pathway for electrons to flow which reduced the current experience by the reactor tube, clearly explaining the loss in performance.
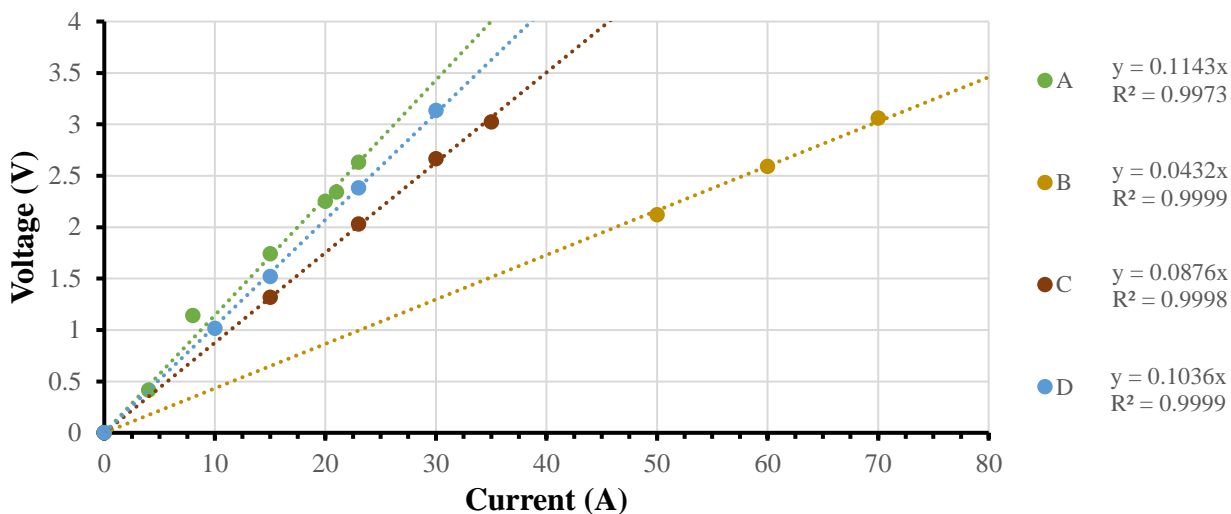

Figure 7. Voltage vs. current curves for the control **(A)** and the reactor system without modification **(B)**, with PTFE bypass line **(C)** and with dielectric fitting **(D)**. Slopes of the fitted lines, represent the resistance of the system.

Although the bypass modification significantly improved the performance of the system, there was still room for improvement. It was suspected that part of the current may be leaking from the system through a ground connection, or some of the connected units may be acting as capacitors. To prevent this, dielectric fittings were installed in the gas lines and all support structure connections were insulation. This provided effective electrical isolation to reach performance very close to the control system. The final results are shown in data set **(D)**. While there is still a small difference between the control and the final modified system, the measured resistance of 0.1036 was within 10% of the control and was actually closer to the manufacturer quoted resistance than the control. The modifications allowed the potential for temperatures of over 1000°C to be reached

while staying well within the power supply's limits and was considered adequate for future experiments.

5.2 CO$_2$ Methanation

Two supported nickel oxide catalysts were tested for CO$_2$ methanation reaction. Since these catalysts had not been previously tested for CO$_2$ methanation, equilibrium concentration and conversion profiles were generated to aid in understanding the thermodynamic limitations of this reaction. These profiles also formed a basis on which experimental results could be compared to determine how closely the reactions were approaching equilibrium. Since forward reaction rates are reduced close to equilibrium, it was important to understand how close to equilibrium the reactions approached. To generate equilibrium data, an equilibrium reactor was implemented in PROII: a chemical process simulation software. The equilibrium reactor was followed by a condenser and flash drum to simulate the condenser in the reactor system where product gases were cooled close to room temperature and the majority of water vapor would be removed.

Measured CO$_2$ effluent concentrations for the Hi-Fuel catalyst compared with equilibrium CO2 concentrations appears to approach equilibrium in **Figure 8 (a)**. However, this due to variation in the other species. Looking at the CO$_2$ conversion for Hi-Fuel in **Figure 8 (b)**, the highest conversion only reaches approximately 75% of the equilibrium conversion. In comparison, WCS shows much lower conversion. The difference in conversion is primarily caused by the use of 2g of Hi-Fuel catalyst vs. 0.2g of WCS. WCS also appears to show higher reaction rates than Hi-Fuel in **Figure 9**. However, the lower approach to equilibrium conversion could explain why it appears to have higher reaction rates than Hi-Fuel. To determine this, an experiment using 0.2g of Hi-Fuel should be conducted in the future to ensure similar residence time.
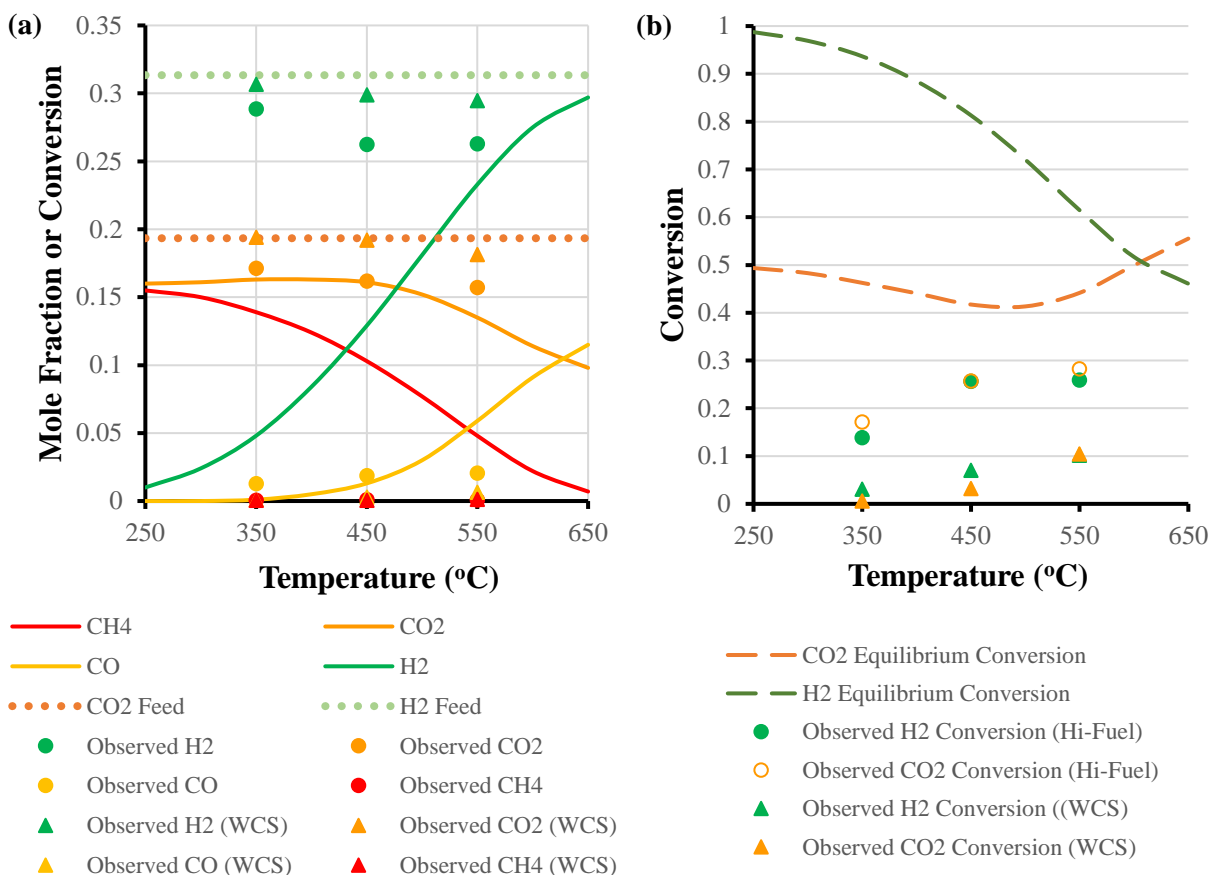
Figure 8. **(a)** Observed product mole fractions for Hi-Fuel (circles) and WCS (triangles) compared to equilibrium values calculated using PROII process simulation software (solid lines). **(b)** Conversions observed for Hi-Fuel (circles) and WCS (triangles) compared

A more significant issue determined from this data set is that GC measurements show significant deviation in the amount of CO_2 that is reacted compared to the amount of carbon products measured. For Hi-Fuel a consistent 70% of the carbon is unaccounted for. WCS shows a 10% carbon deficit at 350°C, a 50% deficit at 450°C and a 70% deficit at 550°C. The deviation at 350°C is likely due to product detection limitations at extremely low conversion of CO_2. The measurement at 450°C also showed low conversion which could explain why it is lower than the other values. If the low conversion cases are thrown out, this system appears to show a consistent 70% deficit of carbon in the products.
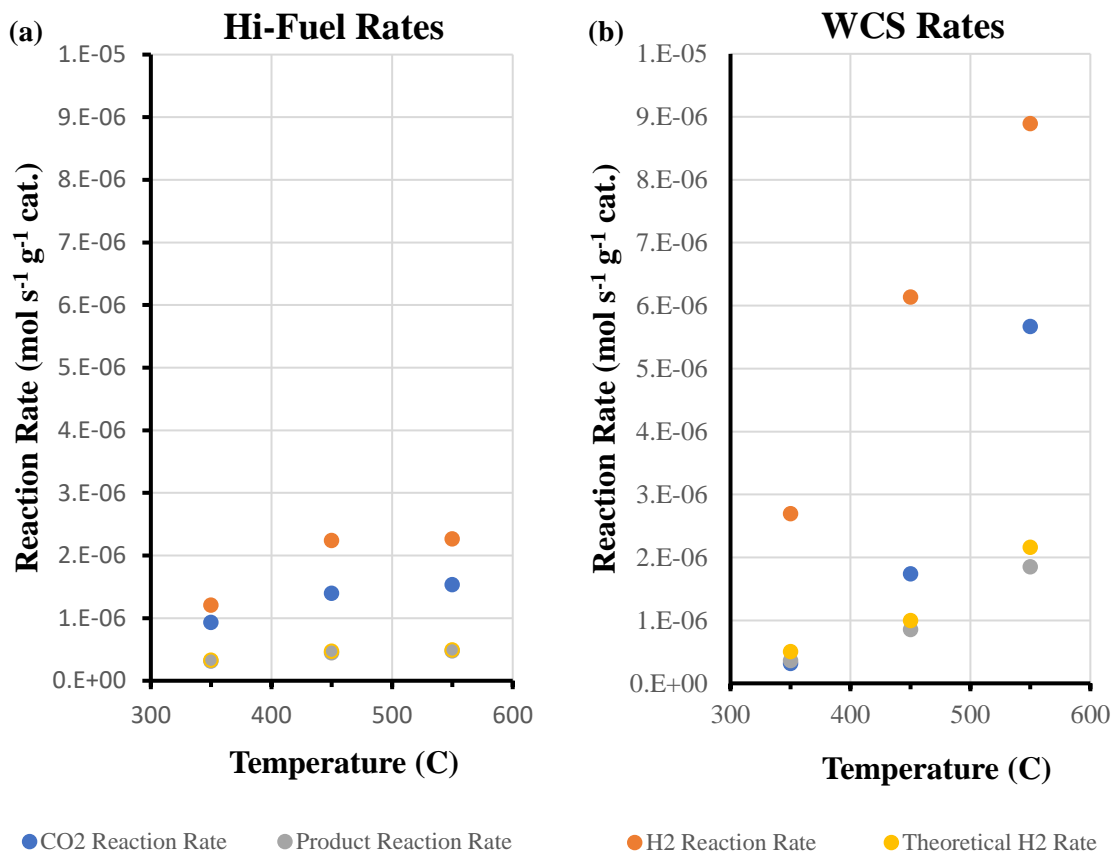
(a) Hi-Fuel Rates

(b) WCS Rates

- CO2 Reaction Rate
- Product Reaction Rate
- H2 Reaction Rate
- Theoretical H2 Rate

Figure 9. Comparison of reaction rates for Hi-Fuel and the WCS. Rates are normalized to the catalyst loading.

Additionally, an unexpectedly high hydrogen reaction rate was observed for all measurements. This can be seen in **Figure 9** where the hydrogen reaction rate predicted from the effluent composition is plotted in yellow. This was calculated using the stoichiometric ratios and observed reaction rates for CO and CH_4. Using this method, the observed hydrogen reaction rates were found to be more than three times the theoretical hydrogen rate. However, a second comparison was made by dividing the hydrogen rate by the CO_2 rate to determine the relationship between hydrogen and carbon on a reactant basis. Values at 350°C and 450°C for WCS are omitted due to product concentrations being too low for the detection limit of the GC, but the 550°C data point again showed agreement with the results of the Hi-Fuel catalyst with Hydrogen to carbon

ratios falling between 1.3 and 1.6. A ratio of 2 would indicate complete conversion to CH_4 whereas a ratio of 1 would indicate complete conversion to CO. The observed hydrogen to carbon ratio suggests that the deficit of carbon products likely accounts for the observed hydrogen reaction rate being too high. Overall, this would suggest that the GC calibration curves used to calculate the CO and CH_4 concentrations should be reexamined, especially at concentrations below 5%.

5.3 Steam Methane Reforming

Results of SMR product concentration measurements were compared to equilibrium concentration curves presented in **Figure 10 (a)** and **(b)**. In both plots, WCS does not show significant deviations in feed concentrations until the temperature is raised to 850°C. In contrast. Hi-Fuel shows noticeable deviations in regard to CH_4, CO_2 and H_2 concentrations. Where CH_4 and CO_2 do not come close to equilibrium concentrations, both WCS and Hi-Fuel show H_2 concentrations exceeding equilibrium concentration for a few higher temperature conditions.

To better understand how close each system was to equilibrium, CH_4 conversion for both Hi-Fuel and WCS operated with furnace supplied heat and Joule heating are plotted in **Figure 11 (a)**. Most conditions showed conversion of CH_4 to be less than 50% which is much less than the 100% equilibrium conversion calculated for these conditions. This indicates that reactions were not likely to be thermodynamically limited for those measurements. However, Joule heating at850^{o}C for WCS and Hi-Fuel, showed conversions of 77% and 79% respectively, so rates for these data points may be suppressed by thermodynamic limitations. Joule heating was also observed to have an overall positive effect on the conversion of CH_4 with improvements increasing with temperature. This is most notable for the 850°C condition where Joule heating shows over twice the conversion observed for the furnace heated system. Lastly, Conversions achieved by WCS are very close to those achieved by Hi-Fuel. Since nearly identical catalyst loadings were
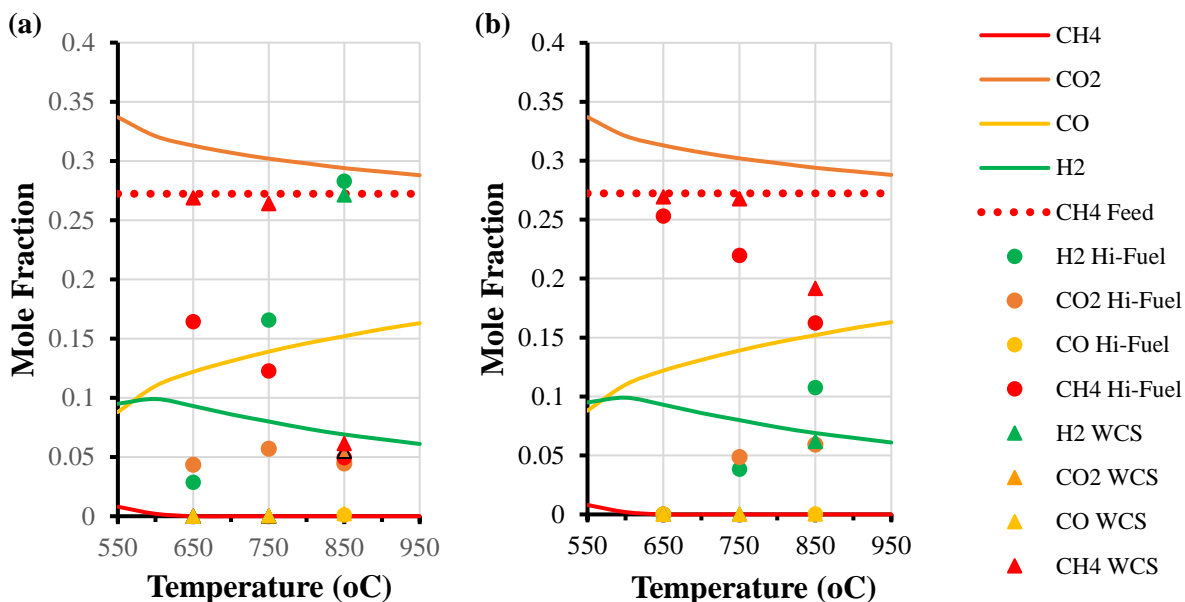
Figure 10. Effluent concentrations compared to calculated equilibrium concentrations. Equilibrium values calculated by PROII are plotted as solid lines. **(a)** Effluent concentrations when heat is provided by the furnace. **(b)** effluent concentrations when heat is provided by Joule heating the reactor tube.

used, (0.2 g of catalyst) this indicates that WCS and Hi-Fuel show similar activity at higher temperatures. Indeed, this is confirmed by comparison of the methane reaction rates for each condition shown in **Figure 11 (b)** where WCS and Hi-Fuel show similar reaction rates under furnace heating and nearly identical rates under Joule heating conditions.

During Joule heating experiments with Hi-Fuel, at 750°C and 850°C, GC responses appeared to be showing decreasing activity over time. Since the current was also being changed over time to maintain constant reactor temperature, it was unclear if this was due to catalyst degradation or the change in current.

To decern if there was a current dependent effect, multiple injections were taken at 750°C with the current decreasing between injections to maintain constant temperature. This resulted in a decrease in current over time which followed the trend of decrease in conversion. The temperature was raised to 850°C and maintained by decreasing current between each injection.
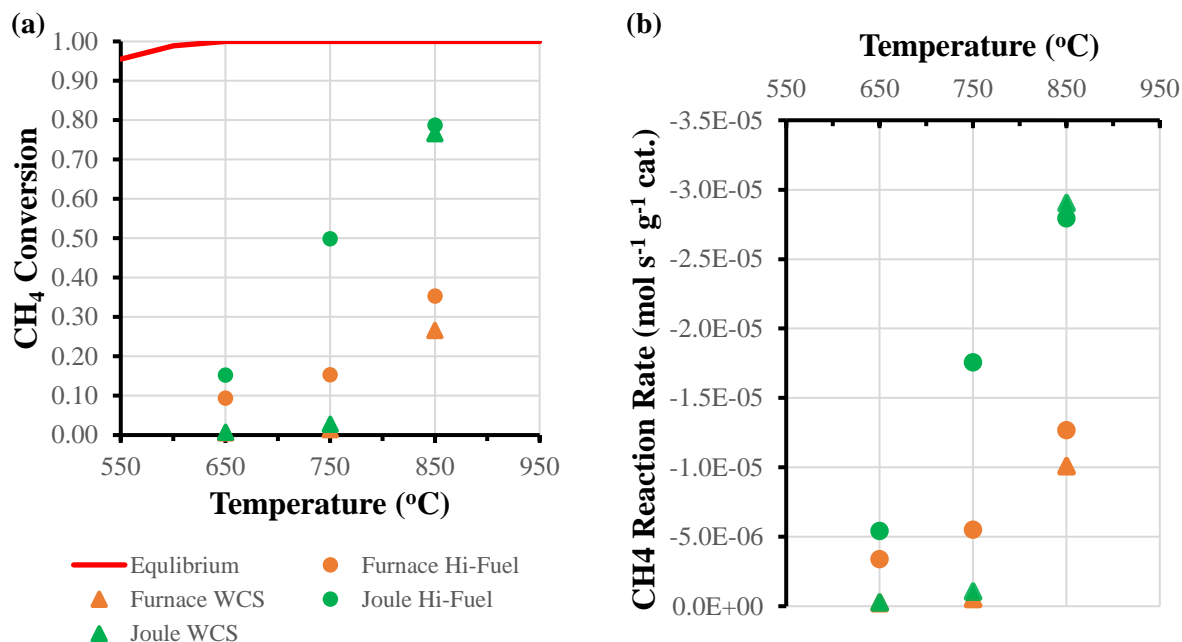
Figure 11. (a) Methane Conversion observed for WCS and Hi-Fuel with furnace and Joule heat compared to the equilibrium conversion calculated by PROII. **(b)** SMR Methane reaction rates observed for WCS and Hi-Fuel with furnace and Joule heat.

Finally, the temperature was decreased to 750°C where the current was increased between injections to maintain constant temperature. Upon increasing the current, it was found that the trend at the previous temperatures was reversed and the conversion increased. The conversion was lower than the previous test at 750°C (30% vs. 50%), but this was also somewhat proportional to the difference in current between the two data sets (38A vs. 49A). Results from this test are highlighted in **Figure 12 (a)** showing the methane conversions and **(b)** showing the reaction rates.
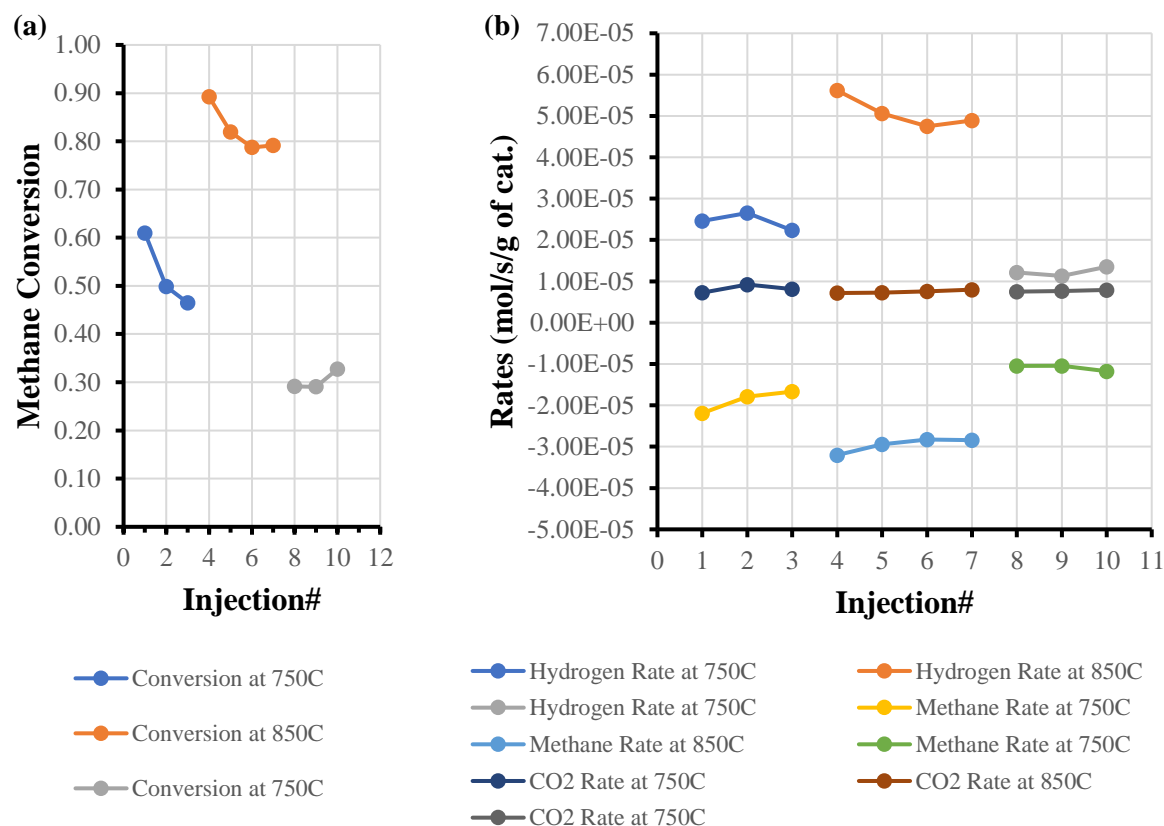
Figure 12. (a) Methane conversions for Hi-Fuel observed at 750°C and 850°C with varying current. **(b)** SMR Reaction rates for Hi-Fuel observed at 750°C and 850°C.

The results of this experiment suggested with more clarity that there may be a correlation between the Joule heating current and the performance of the catalyst. To further investigate this, the method for testing the WCS catalyst for SMR was modified as discussed in the methods section to provide more direct comparison of the catalyst performance under furnace vs Joule heating. Since the WCS did not show significant activity until 850°C, only this temperature was used to test the Joule heating effects in more detail. Initially when heated by the furnace, WCS showed 98% conversion, but this quickly dropped over a few injections to become more stable at low conversion. Once the heating method was switched to Joule heating, the conversion immediately started to increase steadily with increasing current from 30% to over 70% as shown in **Figure 13**.
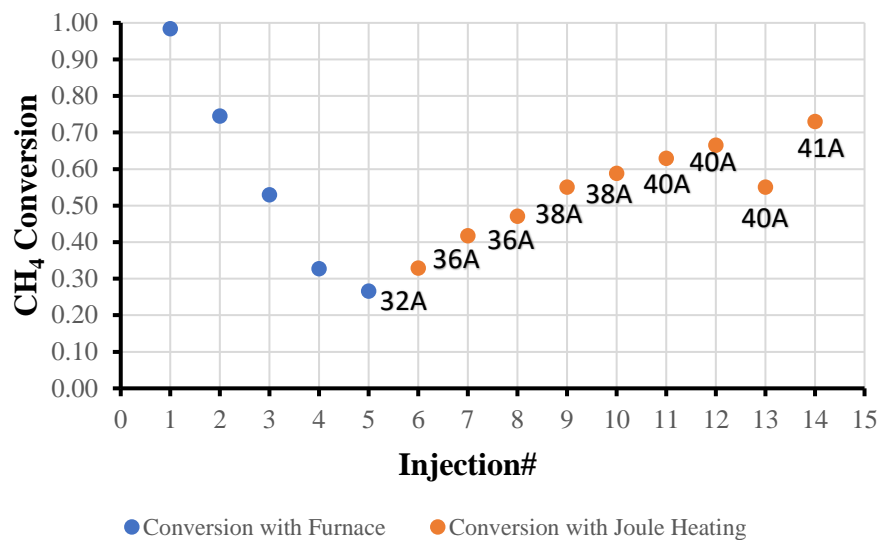
Figure 13. SMR methane conversion for WCS at 850°C initial heated by the furnace, then Joule heated while increasing the current between injections to maintain constant temperature.
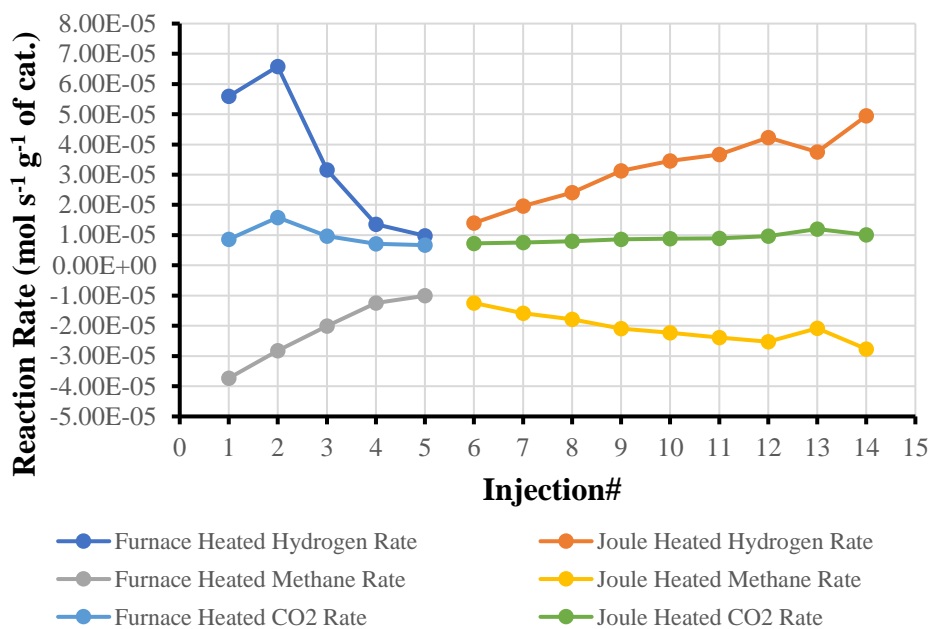

Figure 14. SMR reaction rates for WCS observed at 850°C initial heated by the furnace, then Joule heated while increasing the current between injections to maintain constant temperature.

At injection 13 a dip in performance is clearly seen. I due to the longer length of time that

the system remained at 40 Amps it is likely that this third in injection at 40 Amps is showing the

point at which the positive effects of the increase in current are overcome by the mechanism causing the degradation initially observed. This is also demonstrated by the changes in reaction rates presented in **Figure 14**. Analysis of the H_2 produced per CH_4 reacted provides some insight
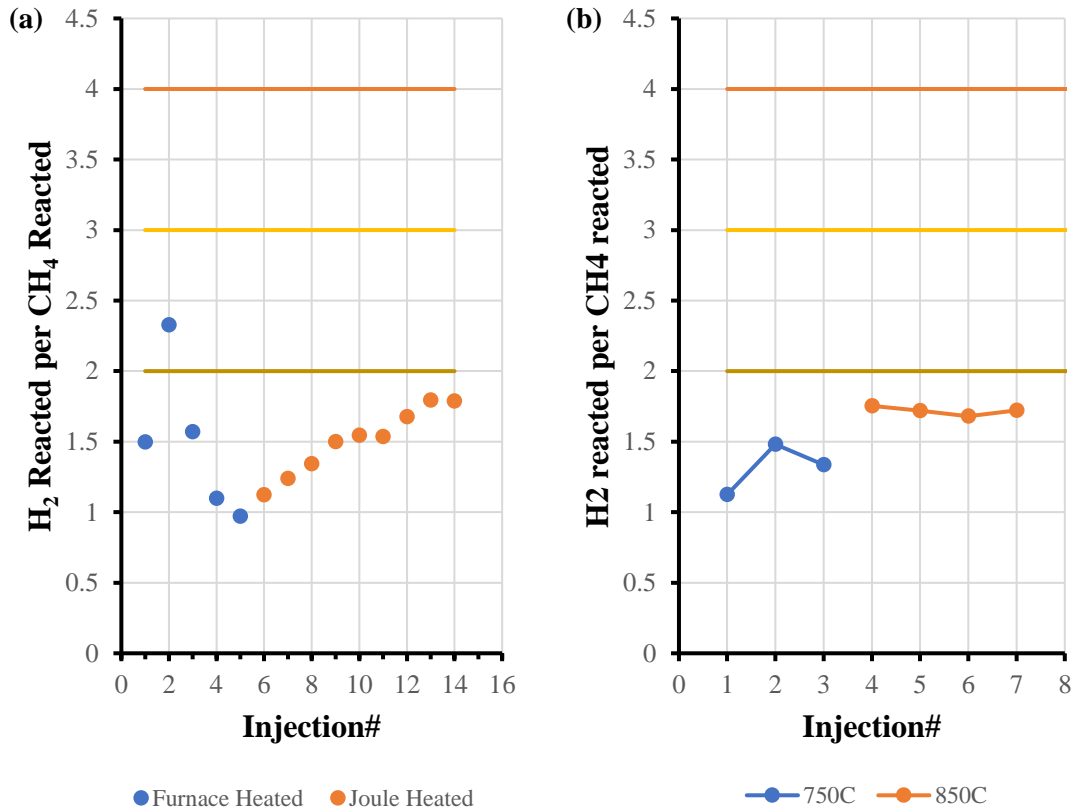

Figure 15. (a) H_2 produced per CH_4 reacted for WCS at 850ºC initial heated by the furnace, then Joule heated while increasing the current between injections to maintain constant temperature. **(b)** H_2 produced per CH_4 reacted for Joule heated Hi-Fuel at 750ºC and 850ºC while increasing current to maintain desired temperature

into what may be causing the overall degradation in performance. Examination of **Figure 15** reveals that the amount of hydrogen produced is far less than would be expected for SMR to CO and CO_2. If SMR were to completely form CO_2 and H2, then an H_2/CH_4 ratio of 4 would be expected, for complete conversion to CO a ratio of 3 would be expected, and if pyrolysis of

methane were to convert methane into carbon and hydrogen a minimum ratio of 2 would be expected.

As seen in **Figure 15 (A)**, the observed ratio is below 2 for most injections which would be most consistent with complex hydrocarbons. This was also observed for the Hi-Fuel experiments shown in **Figure 15 (B)**. Identifying the undesired products being formed would require further characterization, but it is likely that these products are producing coke on the

Figure 16. (a) Close up of black deposits observed on stainless steel rod used to hold catalyst in place. **(b)** Full length of stainless steel rod showing distinct line where the black deposit stops corresponding to the location where joule heating ends

catalyst: which explains the loss of activity. Post experiment, stable and well adhered black deposits were observed on the stainless steel rod used to hold the catalyst in place, further confirming the likelihood of coke formation. **Figure 16** shows the black deposit observed on the rod. The distinct line where the deposit ends corresponds with the exit of the joule heated section of tube. It is unclear what the mechanism allows joule heating to fight this coking degradation, but clearly increasing the current has a positive effect on the catalytic activity while simultaneously

increasing the H_2/CH_4 ratio. Future work will seek to explain this phenomenon from a theoretical perspective.

6. Conclusion

With increasing concerns over chemical manufacturing's environmental impact and a societal shift away from fossil fuels, a future shift in manufacturing technology to electric based systems is likely to occur in the near future. Novel electrochemical processes will likely open new manufacturing pathways due to their unique ability to integrate mass and heat transport on the microscale and to modify the potential of catalytic surfaces. While some of these electrochemical technologies such as water electrolysis and fuel cells are becoming more industrially relevant and economically appealing, many of the desired processes such as electrochemical methane to methanol systems still require significant improvement. A first step for chemical manufacturing processes is to shift methane driven heating systems to renewable based electric heating systems. The basis for using Joule heating in Industry is well established and would offer many benefits over natural gas fired heaters that are currently used in industry. Shifting SMR alone to Joule heating would account for a 1% global reduction in CO_2 emissions. While this technology has long been proposed for industrial application, high electricity prices compared to natural gas have made gas fired heaters the norm. With increased availability of cheap renewable electricity, electricity costs may soon reach a point where Joule heating becomes the more economical option.

This thesis highlights the development of two systems in the Morales-Guio group for investigation of electrically enhances SMR. A reactor testing system based on a ceramic tubular electrochemical reactor architecture has been designed and built to aid in future plans to test high temperatures electrochemical SMR as well as other methane based electrochemical

transformations. Although, no experimentation has been conducted with this setup to date, the successful design and construction of this system is a crucial first step, that will allow testing to commence in the following months. Alongside the development of this electrochemical cell, an existing reactor system was modified to utilize Joule heating and to investigate its effects on CO_2 methanation and SMR. A packed-bed type, commercially available NiO based reforming catalyst (Hi-Fuel) was used as a baseline to which catalyst fabricated in-house could be compared. Also tested was a NiO impregnated ZrO_2 powder that was designed to simulate the catalyst used in a washcoated reactor that would be tested separately. For CO_2 methanation, WCS showed improved reaction rates compared to Hi-Fuel at higher temperatures. When used for SMR, both catalysts showed similar performance at 850°C while Hi-Fuel showed better performance at lower temperatures. In both case for SMR, Joule heating showed significantly improved performance compared to when the reactor was heated externally by the furnace. Coking was observed at high temperature SMR which led to activity loss for both catalysts. However, Joule heating was somehow able to counteract the coking effect and improve the performance compared to furnace heating. Overall, the results of these experiments suggest that Joule Heating has a significant positive effect on the catalyst performance and that the fabricated NiO/ZrO_2 catalyst performance is comparable to that of industrially relevant reforming catalysts. While future, more targeted experiments will be required to understand the fundamental reasoning for Joule heating's performance enhancement, these experiments here have laid the groundwork for future experiment and shown that this kind of experimentation can be successfully conducting by the Morales-Guio group.
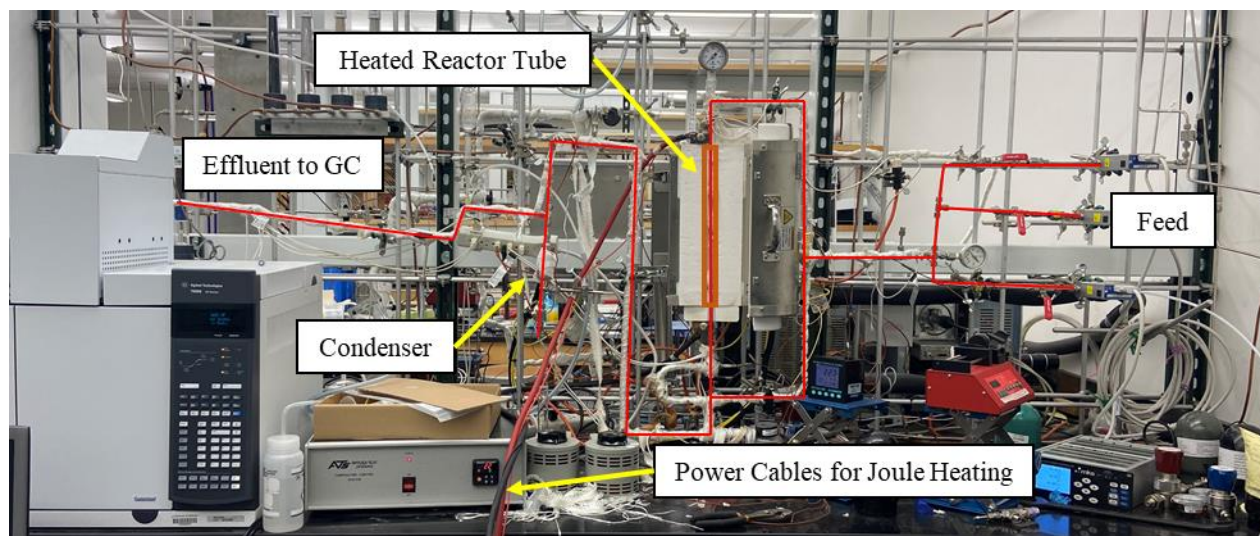
Appendix

Figure 17. An overview picture of the Joule Heated reactor system highlighting key components and gas flow pathways.
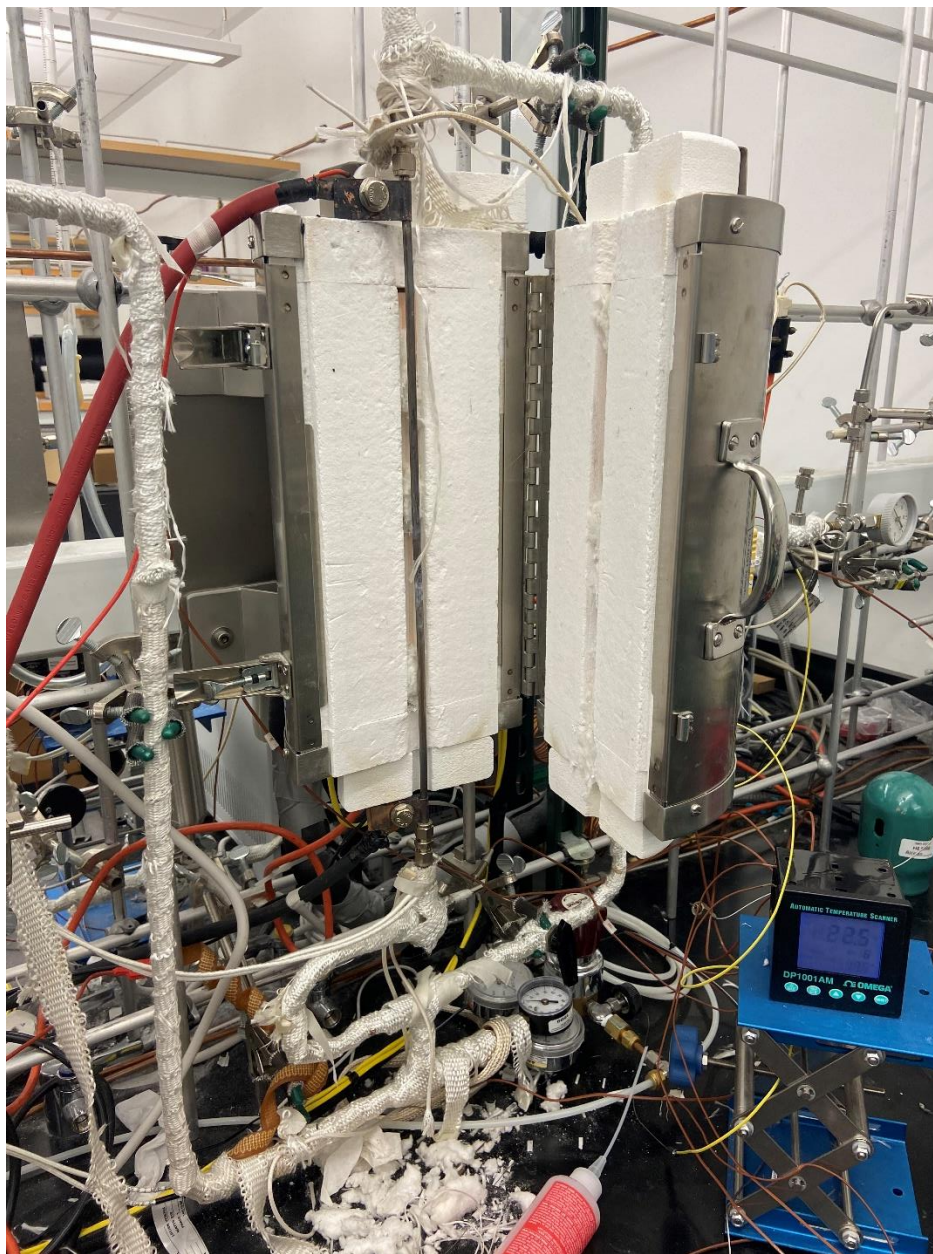
Figure 18. Close up view of Joule heated reactor tube mounted in furnace with power cables attached.
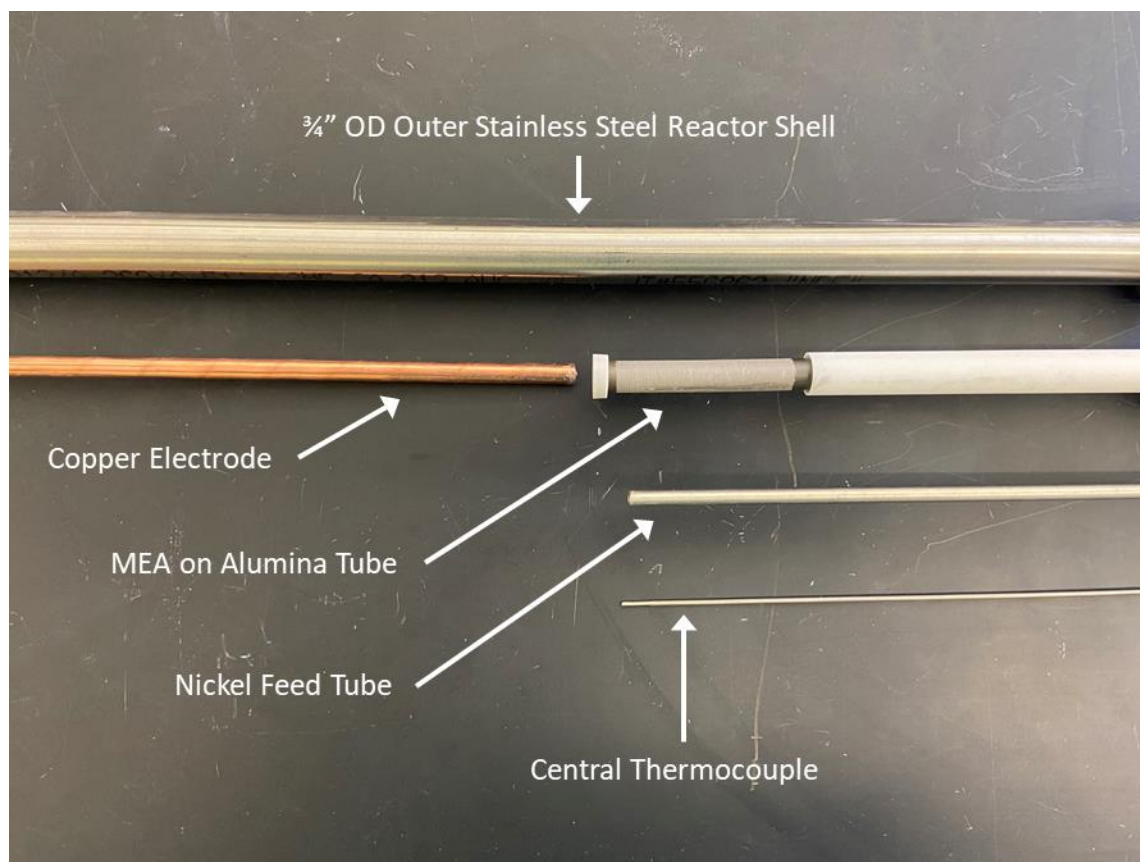
Figure 19. Detailed view of PCMR internal components arranged by location in reactor.

References

1.   Malerød-Fjeld, H. *et al.* Thermo-electrochemical production of compressed hydrogen from methane with near-zero energy loss. *Nature Energy* **2**, 923–931 (2017).

2.   Smith, C., Hill, A. K. & Torrente-Murciano, L. Current and future role of Haber-Bosch ammonia in a carbon-free energy landscape. *Energy and Environmental Science* **13**, 331–344 (2020).

3.   Bagherzadeh Mostaghimi, A. H., Al-Attas, T. A., Kibria, M. G. & Siahrostami, S. A review on electrocatalytic oxidation of methane to oxygenates. *Journal of Materials Chemistry A* **8**, 15575–15590 (2020).

4.   Falter, W., Langer, A., Wesche, F. & Wezel, S. Decarbonization strategies in converging chemical and energy markets. *Journal of Business chemsitry* 20–40 (2019) doi:10.17879/22139481097.

5.   Projected Costs of Generating Electricity 2020 – Analysis - IEA. https://www.iea.org/reports/projected-costs-of-generating-electricity-2020.

6.   Hieminga, G. & Patterson, W. Energy outlook 2021. **2021**, 1–22 (2021).

7.   Bendixen, F. B. *et al.* Industrial Hydrogen Production. *Science* **759**, 756–759 (2019).

8.   Redko, A., Redko, O. & DiPippo, R. Industrial waste heat resources. in *Low-Temperature Energy Systems with Applications of Renewable Energy* 329–362 (Elsevier, 2020). doi:10.1016/b978-0-12-816249-1.00009-1.

9.   Peng, X. D. Analysis of the thermal efficiency limit of the steam methane reforming process. *Industrial and Engineering Chemistry Research* **51**, 16385–16392 (2012).

10.   Simpson, A. P. & Lutz, A. E. Exergy analysis of hydrogen production via steam methane reforming. *International Journal of Hydrogen Energy* **32**, 4811–4820 (2007).

11.   Perkin, R. M. Electrically Generated Heat. *Ullmann's Encyclopedia of Industrial Chemistry* (2000) doi:10.1002/14356007.b03_15.

12.   Rissman, J. *et al.* Technologies and policies to decarbonize global industry: Review and assessment of mitigation drivers through 2070. *Applied Energy* **266**, (2020).

13.   Zhou, L., Guo, Y., Yagi, M., Sakurai, M. & Kameyama, H. Investigation of a novel porous anodic alumina plate for methane steam reforming: Hydrothermal stability, electrical heating possibility and reforming reactivity. *International Journal of Hydrogen Energy* **34**, 844–858 (2009).

14.   Lao, L. *et al.* CFD modeling and control of a steam methane reforming reactor. *Chemical Engineering Science* **148**, 78–92 (2016).

15.   Rostrup-Nielsen, J. R. Steam reforming and chemical recuperation. *Catalysis Today* **145**, 72–75 (2009).

16.   Karim, A., Bravo, J., Gorm, D., Conant, T. & Datye, A. Comparison of wall-coated and packed-bed reactors for steam reforming of methanol. *Catalysis Today* **110**, 86–91 (2005).

17.   Karim, A., Bravo, J. & Datye, A. Nonisothermality in packed bed reactors for steam reforming of methanol. *Applied Catalysis A: General* **282**, 101–109 (2005).

18.   Balzarotti, R., Ambrosetti, M., Beretta, A., Groppi, G. & Tronconi, E. Investigation of packed conductive foams as a novel reactor configuration for methane steam reforming. *Chemical Engineering Journal* **391**, (2020).

19.   Kyriakou, V., Garagounis, I., Vourros, A., Vasileiou, E. & Stoukides, M. An Electrochemical Haber-Bosch Process. *Joule* **4**, 142–158 (2020).

20.   Yuan, S. *et al.* Conversion of Methane into Liquid Fuels—Bridging Thermal Catalysis with Electrocatalysis. *Advanced Energy Materials* **10**, 1–19 (2020).

21.   Latimer, A. A., Kakekhani, A., Kulkarni, A. R. & Nørskov, J. K. Direct Methane to Methanol: The Selectivity-Conversion Limit and Design Strategies. *ACS Catalysis* **8**, 6894–6907 (2018).

22.   Latimer, A. A. *et al.* Mechanistic insights into heterogeneous methane activation. *Physical Chemistry Chemical Physics* **19**, 3575–3581 (2017).

23.   de Rooij, D. M. R. Electrochemical Methods: Fundamentals and Applications. *Anti-Corrosion Methods and Materials* vol. 50 (2003).

24.   Tomita, A., Nakajima, J. & Hibino, T. Direct Oxidation of Methane to Methanol at Low Temperature and Pressure in an Electrochemical Fuel Cell. *Angewandte Chemie International Edition* **47**, 1462–1464 (2008).

25.   Spinner, N. & Mustain, W. E. Electrochemical Methane Activation and Conversion to Oxygenates at Room Temperature. *ECS Transactions* **53**, 1–20 (2013).

26.   Garagounis, I., Vourros, A., Stoukides, D., Dasopoulos, D. & Stoukides, M. Electrochemical synthesis of ammonia: Recent efforts and future outlook. *Membranes* **9**, 1–17 (2019).

27.   Omasta, T. J. *et al.* Two Pathways for Near Room Temperature Electrochemical Conversion of Methane to Methanol. *ECS Transactions* **66**, 129–136 (2015).

28.   Deng, J. *et al.* Ambient methane functionalization initiated by electrochemical oxidation of a vanadium (V)-oxo dimer. *Nature Communications* **11**, 1–10 (2020).

29.   Vøllestad, E. *et al.* Mixed proton and electron conducting double perovskite anodes for stable and efficient tubular proton ceramic electrolysers. *Nature Materials* **18**, 752–759 (2019).

30.   Jang, J., Shen, K. & Morales-Guio, C. G. Electrochemical Direct Partial Oxidation of Methane to Methanol. *Joule* **3**, 2589–2593 (2019).

31.   J. M. Smith, H. C. Van Ness, M. M. A. *Introduction to Chemical Engineering Thermodynamics*. (McGraw-Hill, 2005).

32.   Keith, D. W., Holmes, G., st. Angelo, D. & Heidel, K. A Process for Capturing CO2 from the Atmosphere. *Joule* **2**, 1573–1594 (2018).

33.   Hiller, H., Reimert, R. & Stönner, H.-M. Gas Production, 1. Introduction. in *Ullmann's Encyclopedia of Industrial Chemistry* (Wiley-VCH Verlag GmbH & Co. KGaA, 2011). doi:10.1002/14356007.a12_169.pub3.

34.   Ppl, M. A. X. A. Ammonia , 2 . Production Processes. doi:10.1002/14356007.o02.

35.   Ott, J. *et al.* Methanol. in *Ullmann's Encyclopedia of Industrial Chemistry* (Wiley-VCH Verlag GmbH & Co. KGaA, 2012). doi:10.1002/14356007.a16_465.pub3.

36.   Wei, J. & Iglesia, E. Mechanism and Site Requirements for Activation and Chemical Conversion of Methane on Supported Pt Clusters and Turnover Rate Comparisons among Noble Metals. *Journal of Physical Chemistry B* **108**, 4094–4103 (2004).

37.   Wei, J. & Iglesia, E. Structural and mechanistic requirements for methane activation and chemical conversion on supported iridium clusters. *Angewandte Chemie - International Edition* **43**, 3685–3688 (2004).

38.   Wei, J. & Iglesia, E. Reaction pathways and site requirements for the activation and chemical conversion of methane on Ru-based catalysts. *Journal of Physical Chemistry B* **108**, 7253–7262 (2004).

39.   Wei, J. & Iglesia, E. Structural requirements and reaction pathways in methane activation and chemical conversion catalyzed by rhodium. *Journal of Catalysis* **225**, 116–127 (2004).

40.   Wei, J. & Iglesia, E. Reforming and Decomposition Reactions on Supported Iridium Catalysts. *Phys.Chem.Chem.Phys.* **6**, 3754–3759 (2004).

41.   Wei, J. & Iglesia, E. Isotopic and kinetic assessment of the mechanism of reactions of CH 4 with CO2 or H2O to form synthesis gas and carbon on nickel catalysts. *Journal of Catalysis* **224**, 370–383 (2004).

42.   Meloni, E., Martino, M. & Palma, V. A short review on ni based catalysts and related engineering issues for methane steam reforming. *Catalysts* vol. 10 (2020).

43.   Häussinger, P., Lohmüller, R. & Watson, A. M. Hydrogen, 2. Production. in *Ullmann's Encyclopedia of Industrial Chemistry* (Wiley-VCH Verlag GmbH & Co. KGaA, 2011). doi:10.1002/14356007.o13_o03.

44.   Tong, Y. *et al.* Protonic Ceramic Electrochemical Cell for Efficient Separation of Hydrogen. *ACS Applied Materials and Interfaces* **12**, 25809–25817 (2020).

45.   Duan, C., Huang, J., Sullivan, N. & O'Hayre, R. Proton-conducting oxides for energy conversion and storage. *Applied Physics Reviews* **7**, (2020).

46.   Kee, B. L. *et al.* Thermodynamic insights for electrochemical hydrogen compression with proton-conducting membranes. *Membranes* **9**, (2019).